

Environmental Effect on Evolutionary Cyclic Plasticity Material Parameters of 316 Stainless Steel: An Experimental & Material Modeling Approach

Nuclear Engineering Division

About Argonne National Laboratory

Argonne is a U.S. Department of Energy laboratory managed by UChicago Argonne, LLC under contract DE-AC02-06CH11357. The Laboratory's main facility is outside Chicago, at 9700 South Cass Avenue, Argonne, Illinois 60439. For information about Argonne and its pioneering science and technology programs, see www.anl.gov.

DOCUMENT AVAILABILITY

Online Access: U.S. Department of Energy (DOE) reports produced after 1991 and a growing number of pre-1991 documents are available free via DOE's SciTech Connect (<http://www.osti.gov/scitech/>)

Reports not in digital format may be purchased by the public from the National Technical Information Service (NTIS):

U.S. Department of Commerce
National Technical Information Service
5301 Shawnee Rd
Alexandria, VA 22312
www.ntis.gov
Phone: (800) 553-NTIS (6847) or (703) 605-6000
Fax: (703) 605-6900
Email: **orders@ntis.gov**

Reports not in digital format are available to DOE and DOE contractors from the Office of Scientific and Technical Information (OSTI):

U.S. Department of Energy
Office of Scientific and Technical Information
P.O. Box 62
Oak Ridge, TN 37831-0062
www.osti.gov
Phone: (865) 576-8401
Fax: (865) 576-5728
Email: **reports@osti.gov**

Disclaimer

This report was prepared as an account of work sponsored by an agency of the United States Government. Neither the United States Government nor any agency thereof, nor UChicago Argonne, LLC, nor any of their employees or officers, makes any warranty, express or implied, or assumes any legal liability or responsibility for the accuracy, completeness, or usefulness of any information, apparatus, product, or process disclosed, or represents that its use would not infringe privately owned rights. Reference herein to any specific commercial product, process, or service by trade name, trademark, manufacturer, or otherwise, does not necessarily constitute or imply its endorsement, recommendation, or favoring by the United States Government or any agency thereof. The views and opinions of document authors expressed herein do not necessarily state or reflect those of the United States Government or any agency thereof, Argonne National Laboratory, or UChicago Argonne, LLC.

**Environmental Effect on Evolutionary Cyclic Plasticity Material
Parameters of 316 Stainless Steel: An Experimental & Material
Modeling Approach**

Subhasish Mohanty, William K. Soppet, Saurin Majumdar, and Ken Natesan
Nuclear Engineering Division
Argonne National Laboratory

September 2014

This page intentionally left blank

ABSTRACT

This report provides an update on an earlier assessment of environmentally assisted fatigue for light water reactor (LWR) materials under extended service conditions. This report is a deliverable under the work package for environmentally assisted fatigue in the Light Water Reactor Sustainability (LWRS) program. The overall objective of this LWRS project is to assess the degradation by environmentally assisted cracking/fatigue of LWR materials such as various alloy base metals and their welds used in reactor coolant system piping. This effort is to support the Department of Energy LWRS program for developing tools to understand the aging/failure mechanism and to predict the remaining life of LWR components for anticipated 60-80 year operation. The Argonne National Laboratory work package can broadly be divided into the following tasks:

1. Development of mechanistic-based predictive model for life estimation of LWR reactor coolant system piping material (base and weld metals) subjected to stress corrosion cracking and/or corrosion fatigue
2. Performance of environmentally assisted cracking/fatigue experiments to validate and/or complement the activities on mechanistic model development.

There are a number of subtasks under the above-mentioned major tasks. During the current fiscal year, the following tasks were completed:

1. Fatigue test of
 - a) 316SS base metal specimen under in-air elevated temperature (300 °C) condition, with 0.5% strain amplitude and 0.1%/S strain rate (test number- F06)
 - b) 316SS-316SS pure weld specimen under in-air elevated temperature (300 °C) condition, with 0.5% strain amplitude and 0.1%/S strain rate (test number- F07)
 - c) 316SS-316SS pure weld specimen under in-air room temperature condition, with 0.5% strain amplitude and 0.1%/S strain rate (test number- F08)
 - d) Repeat test of 316SS base metal specimen under in-air room temperature condition, with 0.5% strain amplitude and 0.1%/S strain rate (test number- F09)
 - e) 316SS base metal specimen under in-air room temperature condition, with 0.5% strain amplitude and 0.01%/S strain rate (test number- F10)
 - f) 316SS base metal specimen under elevated temperature (300 °C) and high purity water condition, with 0.136 mm (5.347mil) stroke amplitude and 0.0272 mm/S (1.0694 mil/S) stroke rate (test number- F11)

- g) 316SS base metal specimen under elevated temperature (300 °C) and PWR primary water coolant condition, with 0.136 mm (5.347mil) stroke amplitude and 0.0272 mm/S (1.0694 mil/S) stroke rate (test number- F12)
 - h) 316SS base metal specimen under elevated temperature (300 °C) and in-air condition, with 0.1313 mm (5.1693 mil) stroke amplitude and 0.02626 mm/S (1.0339 mil/S) stroke rate (test number- F13)
 - i) 316SS base metal specimen under elevated temperature (300 °C) and PWR primary water coolant condition, with 0.1313 mm (5.1693 mil) stroke amplitude and 0.02626 mm/S (1.0339 mil/S) stroke rate (test number- F13)
2. Development of evolutionary cyclic plasticity material models with estimation of evolutionary (cycle dependent) elastic material properties, inter cycle isotropic hardening parameters and evolutionary (cycle dependent) linear and nonlinear kinematic parameters for various cases.

The report is organized into two major sections such as:

1. Evolutionary Cyclic Plasticity Model: Theoretic Background for Material Modeling
2. Environmental Fatigue Test of 316SS Specimens & Estimation of Cyclic Plasticity Material Model Parameters under PWR Primary Loop Coolant Water Chemistry

This page intentionally left blank

TABLE OF CONTENTS

ABSTRACT	i
Table of Contents	iv
List of Figures	v
List of TABLES	viii
Abbreviations	ix
Acknowledgments	x
1 Evolutionary Cyclic Plasticity Model: Theoretical Background for Material Modeling	1
1.1 Introduction.....	1
1.2 Cyclic Plasticity Model Generic Background.....	1
1.3 Estimation of Elastic Modulus and Yield Stress Evolution.....	2
1.4 Modeling Evolution of Inter Cycle Yield Stress & Estimation of Isotropic Hardening/Softening Material Parameters.....	3
1.5 Modeling Evolution of Intra Cycle Hardening & Estimation of Kinematic Hardening Material Parameters	7
1.6 Summary	11
2 Environmental Fatigue Test of 316SS Specimens & Estimation of Cyclic Plasticity Material Model Parameters under PWR Primary Loop Coolant Water Chemistry	12
2.1 Introduction.....	12
2.2 Argonne Environmental Test Loop Setup & Test Procedure	12
2.3 PWR Water Condition Fatigue Test (F14): Test Description.....	15
2.3.1 Room temperature pressurization and pressure/flow stabilization of loop	16
2.3.2 Heating up and temperature stabilization of loop	16
2.3.3 Fatigue test under stroke control	22
2.4 F14 Fatigue Test Data Processing & Material Characterization Results.....	26
2.4.1 Time history of stress, stroke, position and strain	26
2.4.2 Evolution of elastic modulus, elastic limit stress, yield stress and accumulated plastic strain	34
2.4.3 Evolution of isotropic hardening stress and estimation of isotropic hardening parameters	37
2.4.4 Evolution of linear kinematic hardening (Prager model) parameters	40
2.4.5 Evolution of nonlinear kinematic hardening (Chaboche model) parameters	42
2.5 Summary	45

LIST OF FIGURES

Figure 1. 1 Equivalent upward and downward monotonic stress strain curves with respect to the corresponding cyclic stress-strain curve	3
Figure 1. 2 Schematic showing isotropic hardening/softening stress evolution.	5
Figure 1. 3 Schematic showing linear vs nonlinear intra cycle hardening stress (kinematic hardening stress) mapping and the evolution of center of yield surface (i.e the back stress)	8
Figure 2. 1 Argonne’s Environmental Fatigue Test System.....	13
Figure 2. 2 a) Close-up view of the pipe autoclave during environmental fatigue test and b) Location of the stroke sensor used for the stroke control environmental fatigue test 13	
Figure 2. 3 a) Close-up view of the dismantled autoclave b) dismantled pull rod and 316SS specimen after failure.....	14
Figure 2. 4 LABVIEW screen shot showing the schematic of various components of test loop	14
Figure 2. 5 LABVIEW screen shot showing the location of heat zone, autoclave inlet and outlet, and location of various thermocouples with respect to autoclave, pull rod, and specimen.....	15
Figure 2. 6 Water temperature versus corresponding water saturation pressure	17
Figure 2. 7 LABVIEW screen shot showing the stroke sensor reading during loop pressurization stage and afterward.....	18
Figure 2. 8 LABVIEW screen shot showing the loop water pressure with respect to time during loop pressurization stage and afterward	18
Figure 2. 9 LABVIEW screen shot showing the frame load sensor reading during loop pressurization stage and afterward.....	18
Figure 2. 10 LABVIEW screen shot showing the frame position sensor reading during loop pressurization stage and afterward.....	19
Figure 2. 11 LABVIEW screen shot showing loop flow sensor reading during loop pressurization stage and afterward.....	19
Figure 2. 12 LABVIEW screen shot showing conductivity (measured through ECP sensor channel & with a multiplication factor of 1e-2) sensor reading during loop pressurization stage and afterward.....	20
Figure 2. 13 LABVIEW screen shot showing TC (from all TC) reading during loop pressurization stage and afterward.....	20
Figure 2. 14 LABVIEW screen shot showing TC (in gauge area) reading during loop pressurization stage and afterward.....	21
Figure 2. 15 LABVIEW screen shot showing TC measurement spatial distribution approximately at 43.96 h.....	21
Figure 2. 16 Stroke strain mapping based on in-air but elevated temperature (300 °C) tensile test data for 316SS specimen	22

Figure 2. 17 LABVIEW screen shot (at the end of test with 3480 fatigue cycle) showing TC (from all TC) reading during main fatigue test.....	23
Figure 2. 18 LABVIEW screen shot (at the end of test with 3480 fatigue cycle) showing TC (from gauge area TC-3, 4 and 5) reading during main fatigue test.....	24
Figure 2. 19 LABVIEW screen shot showing TC measurement spatial distribution approximately at the end of test with 3480 fatigue cycle	24
Figure 2. 20 LABVIEW screen shot (at the end of test with 3480 fatigue cycle) showing the loop water pressure with respect to fatigue cycles during main fatigue test	25
Figure 2. 21 LABVIEW screen shot (at the end of test with 3480 fatigue cycle) showing the loop water flow rate with respect to fatigue cycles during main fatigue test	25
Figure 2. 22 LABVIEW screen shot (at the end of test with 3480 fatigue cycles) showing the loop water conductivity (measured through ECP sensor channel & with a multiplication factor of 1e-2) with respect to fatigue cycles during main fatigue test.....	26
Figure 2. 23 Stroke sensor measurements time history up to first 981 fatigue cycles.....	26
Figure 2. 24 Maximum/minimum stroke amplitude up to 25% load drop (2602 cycles).....	27
Figure 2. 25 Frame position sensor measurements time history up to first 981 fatigue cycles.....	27
Figure 2. 26 Maximum/minimum actuator position up to 25% load drop (2602 cycles).....	28
Figure 2. 27 Frame load cell measurements (stress) time history up to first 981 fatigue cycles.....	28
Figure 2. 28 Magnified view of stress history showing stress hardening and softening	29
Figure 2. 29 Maximum/minimum stress up to 25% load drop (approx. 2602 cycles)	29
Figure 2. 30 Predicted strain time history up to first 981 fatigue cycles	30
Figure 2. 31 Maximum/minimum strain up to 25% load drop (2602 cycles).....	30
Figure 2. 32 Maximum/minimum elastic/plastic strain up to 25% load drop (2602 cycles).....	31
Figure 2. 33 Example of heresies loop (at cycle 1) based on predicted strain using tensile (T04 at 300°C) & cycle test (F13 stroke control, 300°C) parameters	31
Figure 2. 34 Example of heresies loop (at cycle 40) based on predicted strain using tensile (T04 at 300°C) & cycle test (F13 stroke control, 300°C) parameters	32
Figure 2. 35 Example of heresies loop (at cycle 99) based on predicted strain using tensile (T04 at 300°C) & cycle test (F13 stroke control, 300°C) parameters	32
Figure 2. 36 Measured stroke versus stress hysteresis loop up to first 981 fatigue cycle	33
Figure 2. 37 Predicted strain versus stress hysteresis loop up to first 981 fatigue cycle	33
Figure 2. 38 Equivalent quarter cycle predicted strain versus measured stress for estimation of evolutionary material parameters	34
Figure 2. 39 Elevated temperature 300°C tensile test (T04) stress-strain curve showing various elastic and yield limits used as reference in F14 material parameter estimation.....	34
Figure 2. 40 Evolution of elastic modulus for 316SS under PWR condition (as estimated using F14 fatigue test data).....	35
Figure 2. 41 Evolution of elastic limit stress for 316SS under PWR condition	35

Figure 2. 42 Evolution of 0.1% offset yield stress for 316SS under PWR condition..... 36

Figure 2. 43 Evolution of engineering versus true average yield stress (note: true yield stress was used to predict hardening/softening parameters) 36

Figure 2. 44 Evolution of engineering versus true accumulated plastic strain (true plastic stress was used to predict hardening/softening parameters) 37

Figure 2. 45 Evolution of isotropic hardening stress up to 25% load drop (2602 cycles)..... 37

Figure 2. 46 Zoomed version of Figure 2.45 38

Figure 2. 47 Predicted vs. actual isotropic hardening stress 38

Figure 2. 48 Predicted vs. actual isotropic softening stress (up to first 100 cycles)..... 39

Figure 2. 49 Predicted vs. actual isotropic softening stress (up to 25% load drop cycle of 2602) 39

Figure 2. 50 Prager linear kinematic model parameter $C1$ evolution (up to 25% load drop cycle 2602 and with elastic limit stress as offset yield stress) for 316SS under PWR condition 40

Figure 2. 51 Error norm with respect to fatigue cycle while estimating the Prager linear kinematic model parameters shown in Figure 2.50 41

Figure 2. 52 Prager linear kinematic model parameter $C1$ evolution (up to 25% load drop cycle 2602 and with 0.1% offset yield stress) for 316SS under PWR condition..... 41

Figure 2. 53 Error norm with respect to fatigue cycle while estimating the Prager linear kinematic model parameters shown in Figure 2.52 42

Figure 2. 54 Chaboche kinematic model parameter $C1$ evolution (up to 25% load drop cycle 2602 and with elastic limit stress as offset yield stress) for 316SS under PWR condition 42

Figure 2. 55 Chaboche kinematic model parameter $\gamma1$ evolution (up to 25% load drop cycle 2602 and with elastic limit stress as offset yield stress) for 316SS under PWR condition 43

Figure 2. 56 Error norm with respect to fatigue cycle while estimating the Chaboche nonlinear kinematic model parameters shown in Figure 2.54 and Figure 2.55 43

Figure 2. 57 Chaboche nonlinear kinematic model parameter $C1$ evolution (up to 25% load drop cycle 2602 and with 0.1% offset yield stress) for 316SS under PWR condition..... 44

Figure 2. 58 Chaboche nonlinear kinematic model parameter $\gamma1$ evolution (up to 25% load drop cycle 2602 and with 0.1% offset yield stress) for 316SS under PWR condition..... 44

Figure 2. 59 Error norm with respect to fatigue cycle while estimating the Chaboche nonlinear kinematic model parameters shown in Figure 2.57 and Figure 2.58 45

LIST OF TABLES

Table 2. 1 Estimated isotropic hardening parameters (with assumption of 0.1% offset yield stress) for 316SS under PWR condition	40
---	----

ABBREVIATIONS

ANL	Argonne National Laboratory
CF	Corrosion Fatigue
DOE	Department of Energy
FEM	Finite Element Method
LWR	Light Water Reactor
LWRS	Light Water Reactor Sustainability
RT	Room Temperature
ET	Elevated Temperature
SCC	Stress Corrosion Cracking
SS	Stainless Steel

ACKNOWLEDGMENTS

This research was sponsored by the U.S. Department of Energy, Office of Nuclear Energy, for the Light Water Reactor Sustainability Research and Development effort.

1 Evolutionary Cyclic Plasticity Model: Theoretical Background for Material Modeling

1.1 Introduction

In the present work an evolutionary plasticity model is proposed to model LWR coolant system piping materials. In the proposed model it is assumed that the material yield surface and the corresponding hardening and softening behavior evolved over time. It is essential to characterize the behavior under various loading and environmental conditions and then to estimate essential material parameters. These material parameters can be estimated from cyclic stress-strain data obtained through uniaxial fatigue tests conducted under similar environmental conditions and loading envelope. These macroscopic and time-dependent material parameters can be used to develop the component level finite element model of LWR piping components, which in turn can be used for predicting the time-dependent stress-strain behavior under multi-axial thermal-mechanical cyclic loading. In this Section, details of the theoretical background behind the parameters estimation techniques are discussed. In the following Section, the related numerical results will be presented.

1.2 Cyclic Plasticity Model Generic Background

As the material undergoes cyclic loading, the material no more behaves similar as in case of monotonic loading. In cyclic loading the yield surface translates in stress space (kinematic hardening/softening behavior), in addition to its expansion/contraction (isotropic hardening/softening) similar to that in case of monotonic loading. Hence implementation of combined isotropic and kinematic hardening is appropriate for modeling plastic deformation related damage in reactor steel due to cyclic loading. Within an individual cycle, the kinematic hardening is the dominant plastic deformation process, in which the loading surface, the limit surface and the current state depend on the accumulated plastic strain associated with that particular cycle. However, most of this intra cycle hardening can be recovered during stress reversal leading to a dynamic recovery or memory effect (Bauschinger effect). However, over multiple fatigue cycles (inter cycle behavior) the material can also harden or soften due to remnant intra cycle plastic deformation, which can lead to the expansion/contraction of yield surface. This inter cycle expansion/contraction of yield surface is referred as isotropic hardening component in cyclic plasticity model. In the present work, a Von-Mises stress based evolutionary plasticity model is proposed. The corresponding yield function can be expressed as

$$f(\boldsymbol{\sigma}_i^j - \boldsymbol{\alpha}_i^j) = \sigma_i^y \quad 1.1$$

Where, $\boldsymbol{\sigma}_i^j$ is j^{th} instance stress vector in the i^{th} fatigue cycle, whereas $\boldsymbol{\alpha}_i^j$ is corresponding j^{th} instance back stress vector. The back stress vector represents intra cycle memory effect (kinematic hardening stress). In Eq. (1.1) σ_i^y is the i^{th} fatigue cycle yield stress that can be represented through isotropic hardening/softening stress. For pressure independent J2 plasticity the equivalent stress in Eq. (1.1) can be expressed as

$$f(\boldsymbol{\sigma}_i^j - \boldsymbol{\alpha}_i^j) = \sqrt{\frac{3}{2}(\boldsymbol{\sigma}_i^{dev j} - \boldsymbol{\alpha}_i^{dev j}) : (\boldsymbol{\sigma}_i^{dev j} - \boldsymbol{\alpha}_i^{dev j})} \quad 1.2$$

Where, $\boldsymbol{\sigma}_i^{dev j}$ and $\boldsymbol{\alpha}_i^{dev j}$ represent the j^{th} instance deviatoric portion of the primary and back stress vector in the i^{th} fatigue cycle, respectively. To model the cyclic behavior of reactor component it is essential to estimate the cyclic elastic properties (e.g Elastic modulus), back stress vector ($\boldsymbol{\alpha}_i^j$ in Eq. 1.1) and cyclic yield stress (σ_i^y in Eq. 1.1). The cyclic back stress $\boldsymbol{\alpha}_i^j$ can be estimated if the related kinematic hardening material constants are known; whereas the cyclic yield stress can be estimated if the related isotropic hardening material constants are known. These parameters along with cyclic elastic material properties and yield stress can be estimated through cyclic stress-strain data obtained through uniaxial fatigue test. The details of the procedure and theoretical background to estimate these parameters are discussed below.

1.3 Estimation of Elastic Modulus and Yield Stress Evolution

It is essential to know whether or not the elastic properties such as elastic modulus evolve over time due to cyclic loading and how environmental factor affect these parameters. In the present work cycle by cycle elastic modulus is estimated for respective fatigue tests conducted under different environmental conditions. For this purpose, first the cyclic stress-strain curve in each cycle is divided into two half such as upward and downward portion of the stress strain curve as shown in Figure (1.1). Then the divided portions are shifted and scaled (by half) such that the both the curves resemble a tensile test based monotonic stress strain curve. Figure (1.1) shows the example of resulting upward and downward stress-strain curve for a symmetric strain control fatigue test with 0.5 % as maximum strain amplitude. Then from these strain curves the elastic portion (linear portion) of the stress-strain curve is selected based on fixed elastic limit strain. The fixed elastic limits are estimated from monotonic stress-strain data obtained through the tensile test conducted under same strain rate and temperature as the fatigue test of interest. Once the elastic portion of the upward and downward stress-strain curve is selected, the corresponding upward and downward elastic modulus are estimated by using the linear least square technique. These upward and downward elastic constants are averaged to estimate the average elastic modulus in a particular fatigue cycle.

Similar as the cyclic elastic modulus estimation, the 0% offset yield stress (i.e., the stress at elastic limit) and 0.1% offset yield stress are estimated for individual fatigue cycles. To note that automated estimation of offset yield stress requires the knowledge of the corresponding cycle elastic modulus (for slope of the offset intersect line). In the present work although cyclic elastic modulus are estimated, while estimating the cyclic offset yield stress the elastic modulus is assumed fixed and considered same as the elastic modulus obtained from tensile tests conducted under same strain rate and temperature. This is because for simplicity in implementation of cyclic plasticity model through finite element technique, which is currently underway. In addition from the elastic modulus evolution (the results will be discussed in the following

Sections) it is found that the elastic modulus evolution fairly remains stable and use of a fixed elastic modulus would give fairly accurate results.

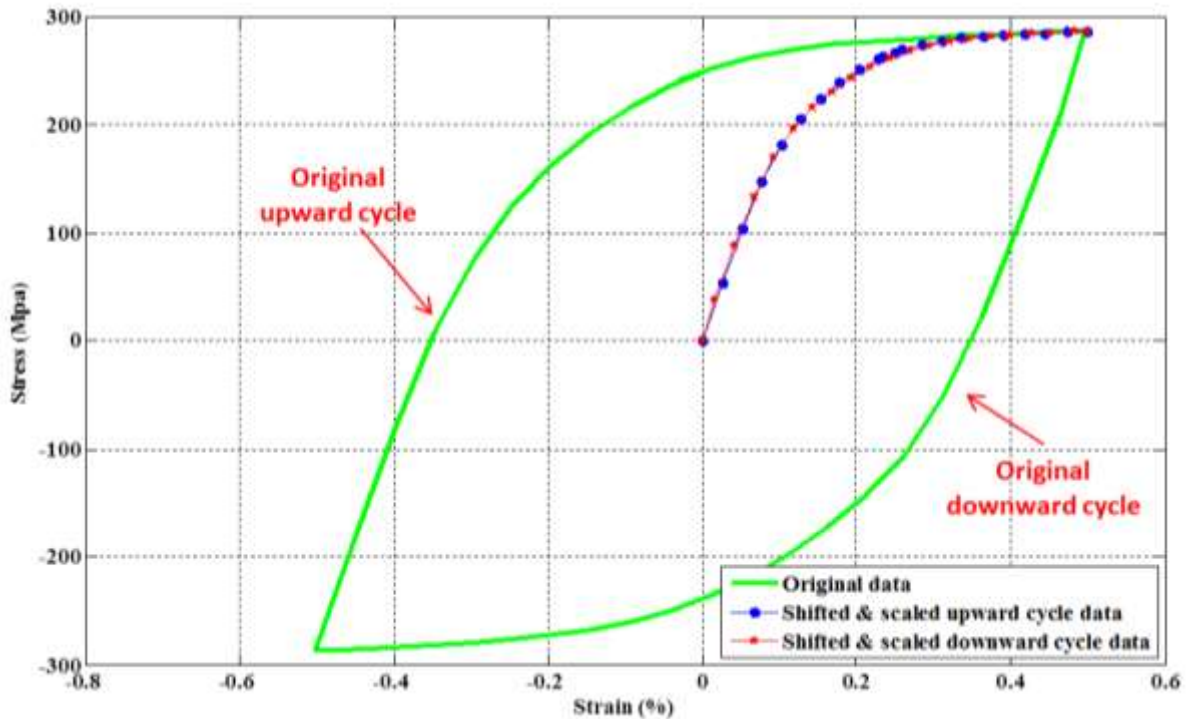


Figure 1. 1 Equivalent upward and downward monotonic stress strain curves with respect to the corresponding cyclic stress-strain curve

1.4 Modeling Evolution of Inter Cycle Yield Stress & Estimation of Isotropic Hardening/Softening Material Parameters

The evolution of yield stress with respect to the fatigue cycles (or with respect to the corresponding accumulated plastic strain) can be modeled using fixed material parameters, known as isotropic hardening parameters. For this purpose, the i^{th} fatigue cycle yield stress in Eq. (1.1) can be expressed using the following expression:

$$\begin{aligned} \sigma_i^y &= \sigma_0^y + R(p_i) \\ \text{or } R(p_i) &= \sigma_i^y - \sigma_0^y \end{aligned} \quad 1.3$$

where, σ_0^y is the 1st quarter cycle yield stress, $R(p_i)$ is the accumulated effective plastic strain (p_i) dependent isotopic hardening/softening stress. The accumulated effective plastic strain can be expressed as

$$p_i = \int_{i=1}^{i=n} dp \quad 1.4$$

For multi-axial case, the effective plastic strain rate can be given as

$$dp = \sqrt{\frac{2}{3}} d\boldsymbol{\varepsilon}^p : d\boldsymbol{\varepsilon}^p \quad 1.5$$

However, for uniaxial case, the effective plastic strain rate can be expressed in terms of cyclic plastic strain range $\Delta\boldsymbol{\varepsilon}_i^{pR}$ as follows:

$$dp = 2\Delta\varepsilon_i^{pR} \quad 1.6$$

whereas the plastic strain range in Eq. 1.6 can be estimated through

$$\Delta\varepsilon_i^{pR} = \left(\varepsilon_i^{\max} - \frac{\varepsilon_i^{\max}}{E_i}\right) - \left(\varepsilon_i^{\min} - \frac{\varepsilon_i^{\min}}{E_i}\right) \quad 1.7$$

In the results discussed in the following Section similar to cyclic yield stress estimation, in Eq. (1.7) a fixed elastic modulus is considered, which is same as the elastic modulus estimated from tensile test under same temperature and strain rate. For isotropic hardening stress, there are many forms to express the evolution of $R(p_i)$ over accumulated cyclic plastic strain p_i (refer to Figure 1.2). In the present work a two stage isotropic hardening/softening model is proposed which is given as below:

$$\begin{aligned} dR(p) &= b^h (Q^{\infty h} - R) dp \quad \text{if } R(p) \leq R^{\max} \quad (\text{hardening}) \\ &= b^s (Q^{\infty s} - R) dp \quad \text{if } R(p) > R^{\max} \quad (\text{softening}) \end{aligned} \quad 1.8$$

where, b^h and $Q^{\infty h}$ are the isotropic hardening parameters, whereas b^s and $Q^{\infty s}$ are the isotropic softening parameters. The corresponding inter cycle plastic strain can be expressed as

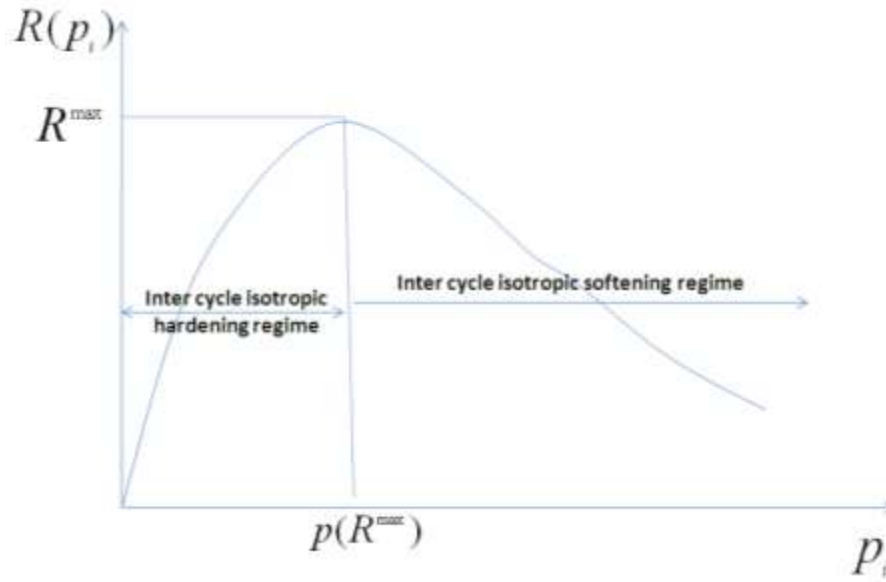


Figure 1. 2 Schematic showing isotropic hardening/softening stress evolution.

$$\begin{aligned}
 p &= \int_0^p dp' && \text{if } R(p) \leq R^{\max} \quad (\text{hardening}) \\
 &= \int_0^p dp' - \int_0^{p(R^{\max})} dp' && \text{if } R(p) > R^{\max} \quad (\text{softening})
 \end{aligned} \tag{1.9}$$

For uniaxial case Eq. (1.8) can be integrated over fatigue cycles as follows

$$\begin{aligned}
 R(p_i) &= \int b^h (Q^{\infty h} - R) dp = Q^{\infty h} [1 - \exp(-b^h p_i)] && \text{if } R(p) \leq R^{\max} \quad (\text{hardening}) \\
 &= \int b^s (Q^{\infty s} - R) dp = Q^{\infty s} [1 - \exp(-b^s p_i)] && \text{if } R(p) > R^{\max} \quad (\text{softening})
 \end{aligned} \tag{1.10}$$

From uniaxial fatigue test data the cyclic isotropic hardening stress R_i for each cycle can be estimated using the cyclic yield stress and the relation given in Eq. (1.3). Whereas the cyclic accumulated plastic strain p_i can be estimated using the cyclic plastic strain range $\Delta \epsilon_i^{pR}$ (Eq. (1.7) and Eq. (1.9)). It is to be noted that, Eq. (1.10) was originally developed to represent an exponential curve (describing only hardening) that saturates with increasing plastic strain. However, in the present work, it will be demonstrated through numerical results (to be discussed in the subsequent Sections), in the cyclic loading case for the present stainless steel material (316 SS nuclear grade), the isotropic hardening stress (i.e., cyclic yield stress with reference to 1st quarter cycle yield stress) increases exponentially to a certain hardening stress (e.g R^{\max} in Figure 1.2), then decreases exponentially to a saturation value before further rapid decrease due

to macroscopic crack initiation. Hence in the present work it is justifiable to separate out the hardening regime from softening regime for accurate representation of material behavior through mechanistic fatigue modeling.

Once the $R_i \sim p_i$ data estimated from a particular fatigue test data set (up to a particular fatigue cycles of interest), then the respective cycle by cycle hardening ($b^h, Q^{\infty h}$) and softening ($b^s, Q^{\infty s}$) parameters can be estimated using curve fitting. The complex nonlinear relation between R_i and p_i , the fitting parameters (e.g. $b^h, Q^{\infty h}$ and $b^s, Q^{\infty s}$) can be estimated using a nonlinear parameter optimization techniques. In the present work a Gauss-Newton type optimization technique is used to estimate the above mentioned hardening/softening parameters. The numerical steps involved are briefly described below:

Step 1: Estimate the cycle by cycle isotropic hardening/softening stress and corresponding accumulated inter cycle plastic strain up to the particular cycle of interest.

Step 2: Assume initial values for $\mathbf{L} = [Q^\infty \ b]^T$

Step 3: Estimate the residual function vector

$$\mathbf{r} = [r_{i=1} \ r_{i=2} \ \cdots \ r_{i=n}]^T \quad 1.11$$

with i^{th} cycle residual as

$$r_i = Q^\infty [1 - \exp(-b \ p_i)] - R_i \quad 1.12$$

Step 4: Estimate the Jacobian matrix \mathbf{J} as follows:

$$\mathbf{J} = \begin{bmatrix} \frac{\partial r_{i=1}}{\partial Q^\infty} & \frac{\partial r_{i=1}}{\partial b} \\ \frac{\partial r_{i=2}}{\partial Q^\infty} & \frac{\partial r_{i=2}}{\partial b} \\ \vdots & \vdots \\ \frac{\partial r_{i=n}}{\partial Q^\infty} & \frac{\partial r_{i=n}}{\partial b} \end{bmatrix} \quad 1.13$$

where the i^{th} cycle expression for the partial derivatives are given below

$$\frac{\partial r_i}{\partial Q^\infty} = 1 - \exp(-b p_i)$$

and

$$\frac{\partial r_i}{\partial b} = Q^\infty b \exp(-b p_i)$$
1.14

Step 5: Estimate the incremental change in parameters:

$$\Delta \mathbf{L} = [\Delta Q^\infty \quad \Delta b]^T = -[(\mathbf{J}^T \mathbf{J})^{-1} \mathbf{J}^T] \mathbf{r}$$
1.15

Step 6: Update the parameters as:

$$\mathbf{L} = [Q^\infty \quad b]^T = \mathbf{L} + \Delta \mathbf{L}$$
1.16

Step 7: Repeat step 3 to step 6 unless the L_2 norm of the incremental parameters $\Delta \mathbf{L}$ less than a tolerance value, i.e.,

$$\|\Delta \mathbf{L}\|_2 \leq t_{tol}$$
1.17

Note that for all the results discussed in this report, a tolerance value of $t_{tol} = 10^{-6}$ was considered.

1.5 Modeling Evolution of Intra Cycle Hardening & Estimation of Kinematic Hardening Material Parameters

The kinematic hardening material parameters are required to model the intra cycle hardening stress such as back stress in material due to loading/unloading within a fatigue cycle. At a given instant (say j^{th} instance) within a particular fatigue cycle (say i^{th} cycle) the back stress $\boldsymbol{\alpha}_i^j$ (refer to Eq. 1.1) has to be estimated in a finite element code. The evolution of the intra cycle hardening stress beyond the corresponding cycle yield stress is equivalent of the evolution of the center of the yield surface in form of back stress $\boldsymbol{\alpha}_i^j$ (refer Figure 1.3). The intra cycle back stress is dependent on accumulated plastic strain within a cycle as well as on some material parameters known as kinematic hardening parameters. These predetermined parameters can be used for modeling cyclic evolution of back stress in a finite element code.

Unlike the monotonic loading case where a fixed set of parameters can completely describe the hardening/softening behavior for entire loading envelope, for cyclic loading case it may not be the case. Due to the cyclic dependency of material deformation, the kinematic hardening behavior within all cycles may not be represented by a single set of kinetic hardening parameters. Rather the kinematic hardening parameters may evolve over time. Hence, it is essential to understand, how these macroscopic hardening parameters evolve over time and how it is affected by different loading conditions (e.g. load amplitude, loading rate) and environmental conditions (e.g. room temperature versus elevated temperate, in-air condition versus light water reactor coolant chemistry condition, etc.). As seen in Fig. 1.3 within a cycle, the stress (beyond the corresponding cycle yield stress, σ_i^y) can be described either by using a linear or a nonlinear mapping of accumulated plastic strain within that cycle.

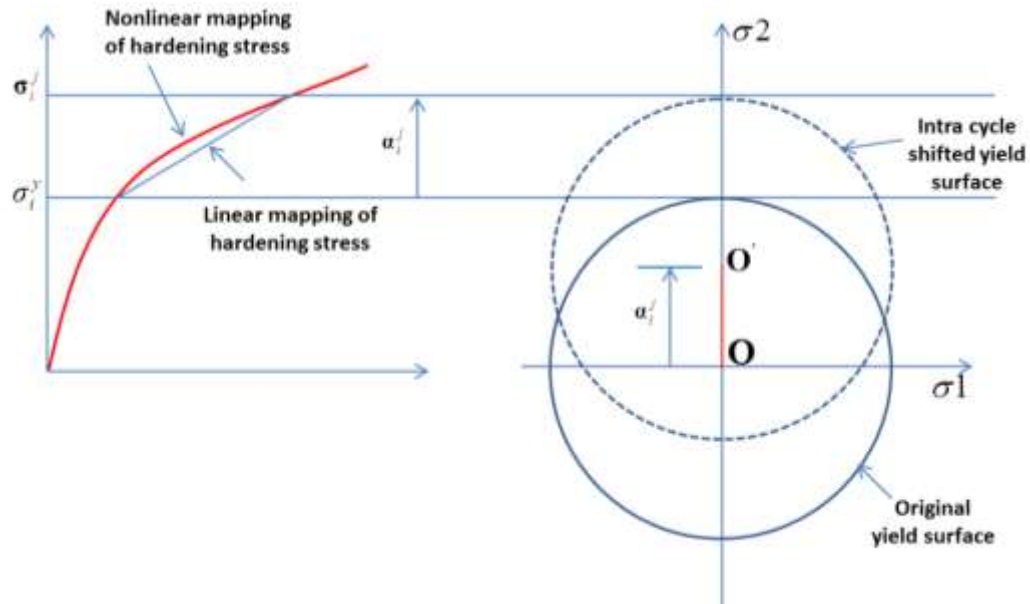


Figure 1.3 Schematic showing linear vs nonlinear intra cycle hardening stress (kinematic hardening stress) mapping and the evolution of center of yield surface (i.e the back stress)

In the present work, the intra cycle kinematic hardening stresses are mapped both linearly and nonlinearly. The linear model is based on Prager's linear hardening relation between hardening stress and accumulated plastic strain, whereas the nonlinear model is based on Armstrong-Frederick or Chaboche nonlinear kinematic hardening relation between hardening stress and accumulated plastic strain. To note that, the original Prager or Chaboche model and other related models suggest to estimate the related kinematic hardening parameters using either 1st quarter cycle or a stabilized cycle stress-strain data. That means the kinematic hardening parameters will remain same over the entire fatigue cycles. However, in reality these parameters may not remain constant rather evolve over time. For this purpose, in the present work a modified linear and nonlinear hardening mapping relations are proposed, according to which the incremental back stress at j^{th} instance in i^{th} fatigue cycle can be expressed as:

$$d\alpha_i^j = \frac{2}{3} C1_i^{av}(p) d\epsilon^{pl} \quad \leftarrow \text{Linear kinematic hardening} \quad 1.18$$

$$d\alpha_i^j = \frac{2}{3} C1_i^{av}(p) d\epsilon^{pl} - \gamma1_i^{av}(p) \alpha_i^j \bar{p} \quad \leftarrow \text{Nonlinear kinematic hardening} \quad 1.19$$

where $\bar{p} = \int_0^{d\epsilon^{pl}} d\epsilon^{pl}$ represents the accumulated plastic strain within a cycle. Whereas the

$C1_i^{av}(p)$ and $\gamma1_i^{av}(p)$ are fatigue cycle or inter cycle accumulated plastic strain (p) dependent material constants. The parameter $C1_i^{av}$ is the proportional constant that gives a linear relation between back stress α_i^j and intra cycle accumulated plastic strain \bar{p} , whereas $\gamma1_i^{av}$ is the

relaxation term that describes the rate at which the back stress decreases with increase in intra cycle accumulated plastic strain \bar{p} . These parameters are to be averaged over the parameters estimated through corresponding upward and downward portions of a symmetric cycle stress-strain curve and can be separated once it is shifted and scaled as described through Figure (1.1). The average kinematic hardening parameters can be expressed as

$$C1_i^{av}(p) = \frac{1}{2}[C1_i^{up}(p) + C1_i^{down}(p)] \quad 1.20$$

and

$$\gamma1_i^{av}(p) = \frac{1}{2}[\gamma1_i^{up}(p) + \gamma1_i^{down}(p)] \quad 1.21$$

Equations (1.18 and 1.19) give the multi-axial representation of intra cycle kinematic hardening stress or back stress. The equivalent uniaxial form can be integrated over a given cycle to estimate the corresponding cycle parameters ($C1_i^{up}$ and $\gamma1_i^{up}$ or $C1_i^{down}$ and $\gamma1_i^{down}$) by curve fitting the stress-strain data obtained in a fatigue test. For example for the upward portion of the hysteresis curve, the integrated form of the Eqs. (1.18) and (1.19) can be written as:

$$\begin{aligned} \alpha_i^j &= \int_0^{\bar{p}} d\alpha_i^j = \int_0^{\bar{p}} \frac{2}{3} C1_i^{up}(p) d\epsilon^{pl} \\ &= \frac{2}{3} C1_i^{up}(p) \bar{p} \quad \leftarrow \text{Linear kinematic hardening} \end{aligned} \quad 1.22$$

$$\begin{aligned} \alpha_i^j &= \int_0^{\bar{p}} d\alpha_i^j = \int_0^{\bar{p}} \left[\frac{2}{3} C1_i^{up}(p) - \gamma1_i^{up}(p) \alpha_i^j \right] d\epsilon^{pl} \\ &= \frac{C1_i^{up}(p)}{\gamma1_i^{up}(p)} [1 - \exp(-\gamma1_i^{up}(p) \bar{p})] \quad \leftarrow \text{Nonlinear kinematic hardening} \end{aligned} \quad 1.23$$

Similarly the bottom half of the cyclic stress-strain curve can model in terms of $C1_i^{down}(p)$, $\gamma1_i^{down}(p)$ and \bar{p} . By using upward and downward portions of a cyclic stress-strain data and using a nonlinear optimization technique such as Gauss-Newton approach all the above-mentioned hardening parameters can be estimated. Below lists the steps for estimating the parameters using Gauss-Newton approach. For a given cycle (say i^{th} cycle):

Step 1: Estimate the kinematic hardening stress and corresponding accumulated intra cycle plastic strain for all the instances ($j = 1, 2, \dots, m$) using

$$\alpha_i^{j=1,2,\dots,m} = \sigma_i^j - \sigma_i^y \quad 1.24$$

$$\bar{p}_i^j = \epsilon_i^j - \frac{\sigma_i^j}{E_i} \quad 1.25$$

where, subscript i represents i^{th} fatigue cycle, superscript j represents j^{th} data point in i^{th} fatigue cycle shifted and scaled stress-strain curve and σ_i^y is the i^{th} fatigue cycle yield stress. In Eq. (1.25) E_i represents the i^{th} fatigue cycle elastic modulus. Note that similar to the case of isotropic hardening parameter estimation, in this case also a fixed elastic modulus is used for the numerical results discussed in the later part of this report. Again this is to simplify for future implementation of proposed hardening model in finite element code although the evolution of E_i is estimated and presented in this report.

Step 2: Assume initial values for $L = [C1_i \ \gamma1_i]^T$

Step 3: Estimate the residual function vector

$$\mathbf{r} = [r^{j=1} \ r^{j=2} \ \dots \ r^{j=m}]^T \quad 1.26$$

with j^{th} instance residual as

$$r^j = \frac{C1_i}{\gamma1_i} [1 - \exp(-\gamma1_{ii} \bar{p}_i^j)] - \alpha_i^j \quad 1.27$$

Step 4: Estimate the Jacobian matrix \mathbf{J} as follows:

$$\mathbf{J} = \begin{bmatrix} \frac{\partial r^{j=1}}{\partial C1_i} & \frac{\partial r^{j=1}}{\partial \gamma1_i} \\ \frac{\partial r^{j=2}}{\partial C1_i} & \frac{\partial r^{j=2}}{\partial \gamma1_i} \\ \vdots & \vdots \\ \frac{\partial r^{j=m}}{\partial C1_i} & \frac{\partial r^{j=m}}{\partial \gamma1_i} \end{bmatrix} \quad 1.28$$

Note that although Eqs. (1.13) and (1.28) look similar, the reader should be careful in distinguishing the use of subscript i (that represents i^{th} fatigue cycle), and superscript j (that represents j^{th} data point within i^{th} fatigue cycle). In Eq. (1.28) the j^{th} instance expression for the partial derivatives are as below

$$\frac{\partial r^j}{\partial C1_i} = \frac{1}{\gamma1_i} [1 - \exp(-\gamma1_{ii} \bar{p}_i^j)] \quad \text{and} \quad 1.29$$

$$\frac{\partial r^j}{\partial \gamma1_i} = -\frac{C1_i}{\gamma1_i^2} [1 - \exp(-\gamma1_{ii} \bar{p}_i^j)] + \frac{\bar{p}_i^j}{\gamma1_i} \exp(-\gamma1_{ii} \bar{p}_i^j)$$

Step 5: Estimate of incremental change in parameters:

$$\Delta \mathbf{L} = [\Delta C1_i \quad \Delta \gamma 1_i]^T = -[(\mathbf{J}^T \mathbf{J})^{-1} \mathbf{J}^T] \mathbf{r} \quad 1.30$$

Step 6: Update the parameters as:

$$\mathbf{L} == [C1_i \quad \gamma 1_i]^T = \mathbf{L} + \Delta \mathbf{L} \quad 1.31$$

Step 7: Repeat step 3 to step 6 unless the L_2 norm of the incremental parameters $\Delta \mathbf{L}$ less than a tolerance value, i.e.,

$$\| \Delta \mathbf{L} \|_2 \leq t_{tol} \quad 1.32$$

Note that for all the results discussed in this report, a tolerance value of $t_{tol} = 10^{-9}$ was considered.

1.6 Summary

In the present Section, the theoretical background behind the estimation of cyclic evolution of elastic modulus, yield stress, isotropic and kinematic hardening parameters is presented. In the subsequent Sections the related numerical results will be presented.

2 Environmental Fatigue Test of 316SS Specimens & Estimation of Cyclic Plasticity Material Model Parameters under PWR Primary Loop Coolant Water Chemistry

2.1 Introduction

In PWRs, the steels used in coolant system components are exposed to PWR coolant water chemistry in addition to the elevated temperature and thermal-mechanical cyclic load. Therefore, the macroscopic material parameters such elastic modulus, yield stress, kinematic and isotropic hardening parameters also may change in comparison with corresponding in-air conditions. For accurate environmental fatigue assessment and/or modeling of reactor components, it is necessary to estimate those parameters under prototypical conditions. For this purpose, several fatigue tests were conducted at the Argonne's environmental fatigue loop under PWR water conditions. The corresponding cycle by cycle test data (e.g. stress, stroke, etc.) were analyzed and processed using the previously discussed method to estimate the evolution of elastic modulus, yield stress, kinematic and isotropic hardening parameters. The details of the environmental fatigue test (EFT) procedure, processed test measurements, and estimated parameters are discussed below.

2.2 Argonne Environmental Test Loop Setup & Test Procedure

At Argonne's nuclear engineering division a dedicated test facility developed/augmented to perform fatigue crack test under light water reactor type conditions (such as temperature, pressure, and water chemistry). The individual components of the test loop can be seen from Figure 2.1. The test loop contains a metallic pipe autoclave, to perform simulated LWR condition fatigue test under high pressure and temperature. Figure 2.2a shows the location of the autoclave, heat exchanger, and autoclave preheater, and Figure 2.2b shows the close of stroke sensor used for controlling the environmental fatigue test. Figure 2.3a and 2.3b, respectively, show the dismantled autoclave and failed specimen with pull rod. During the test, the load/displacement passes to the specimen through the pull rods (top and bottom), while part of both the top and bottom pull rods along with whole specimen stay inside the water-tight autoclave. Since extensometer could not be placed inside the autoclave for strain control fatigue test, the frame was controlled using an external stroke displacement sensor under fatigue loading. The stroke sensor measures the crosshead displacement of test frame. While test was conducted various measurements, such as from thermocouples, load cells, stroke sensor, frame actuator position, loop water pressure, water flow rate, and water conductivity, are made through a LABVIEW based data acquisition system. Figure 2.4 shows the snap shot of LABVIEW window at a given instant of time showing the schematic of overall test loop. Figure 2.5 shows similar LABVIEW window showing the schematic of inlet and outlet of the autoclaves, heating zone (of autoclave through external coils), and some of the thermocouple measurement locations with respect to the pull rod, specimen, and autoclave.

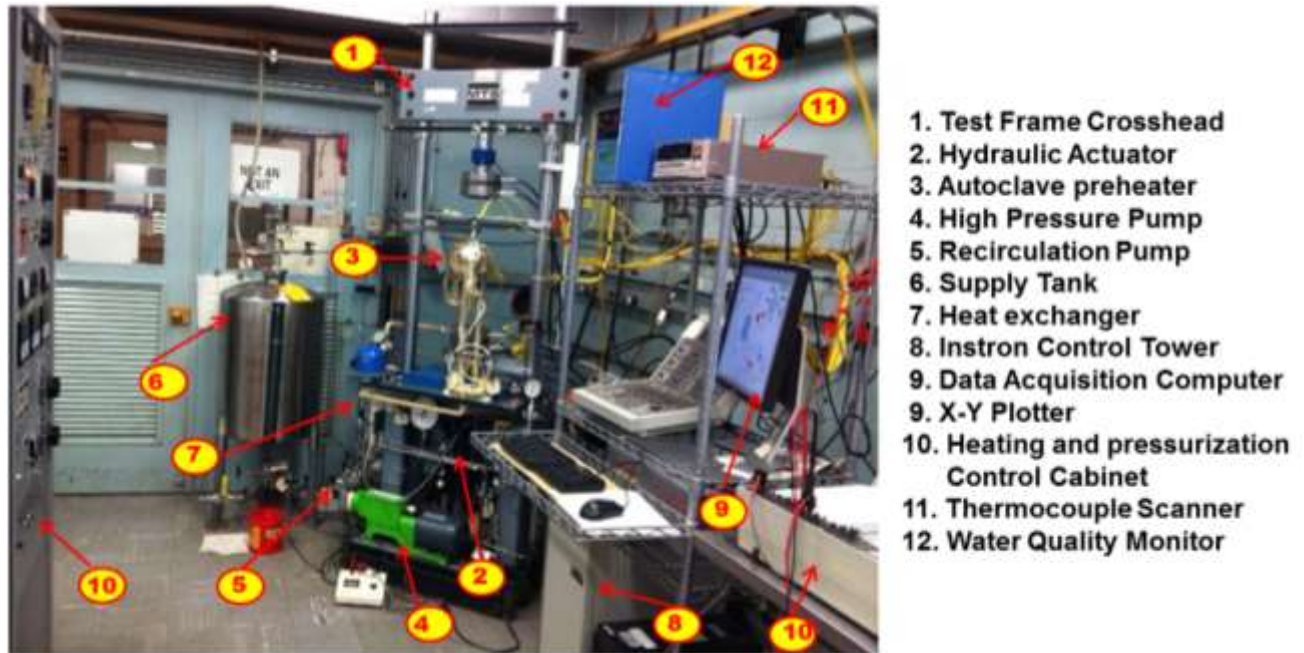


Figure 2. 1 Argonne's Environmental Fatigue Test System

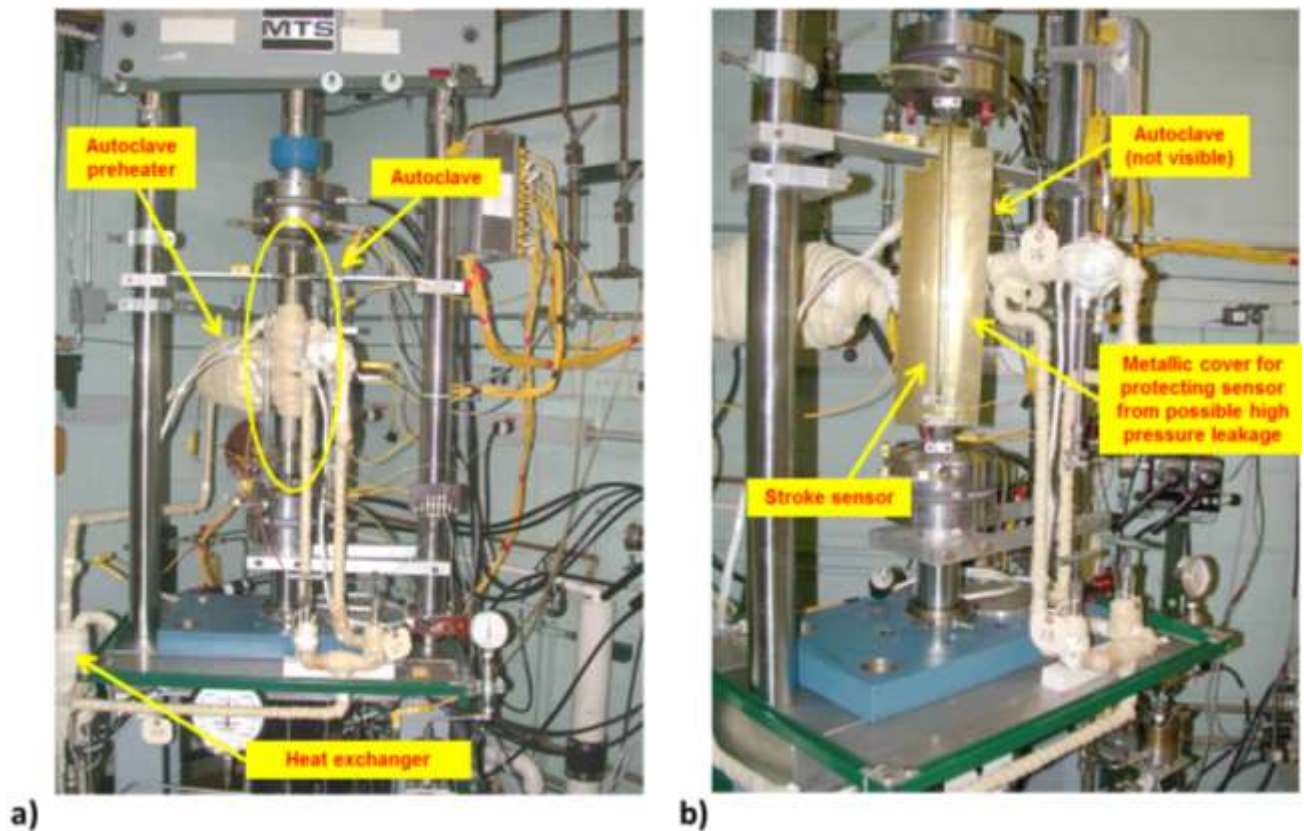


Figure 2. 2 a) Close-up view of the pipe autoclave during environmental fatigue test and b) Location of the stroke sensor used for the stroke control environmental fatigue test

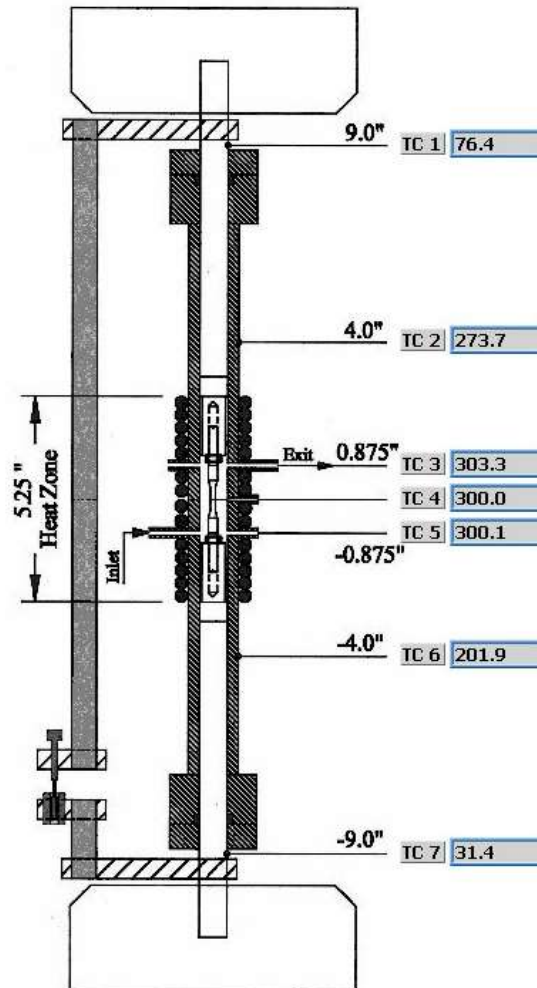


Figure 2. 5 LABVIEW screen shot showing the location of heat zone, autoclave inlet and outlet, and location of various thermocouples with respect to autoclave, pull rod, and specimen

2.3 PWR Water Condition Fatigue Test (F14): Test Description

The test F14 was conducted under PWR water condition, with gauge area target temperature of 300°C, water chemistry: 1000 ppm B as H₃BO₃, 2ppm Li⁺ as LIOH, 20% H₂/Bal N₂ cover gas and DO < 5ppb, approximate Ph 6.3, conductivity ≤ 23 uS/cm. The test was conducted in four stages such as

- Initial room temperature pressurization and pressure stabilization stage under stroke control
- Heating up (to 300°C at gage area) and temperature stabilization stage under load control
- Main fatigue test under stroke control
- Cool down and unloading

Results from the first three stages are briefly discussed below. If required these results can be correlated with material characterization results, which will be discussed in the following Section.

2.3.1 *Room temperature pressurization and pressure/flow stabilization of loop*

During this stage, the loop was pressurized under room temperature condition. The water was pressurized using the high-pressure pump (Figure 2.1) such that the water pressure in the loop would be approximately 1500 psi (10.34 MPa). This was little above the saturation temperature of water (Figure 2.6) at 300°C (572°F) i.e., approximately 1250 psi (8.61 MPa). During this stage, the test frame was in stroke control mode and the controller was set to stay with the original stroke value. Figure 2.7 shows the corresponding crosshead stroke (Figure 2.2b) sensor measurement history for the entire pressurization and pressure/flow stabilization stage (up to approximately 22nd hour) and heating up stage beyond 22nd hour.

The reason for stroke control mode was to avoid straining of specimen due to pressurization. Figure 2.8 shows the LABVIEW screen shot showing the loop water pressure with respect to time during loop pressurization and afterward. After pressure reached the desired value, the test pressure was maintained for a period of approximately 20 hours (in this case approximately up to 21-22nd hour from the start of the test) for pressure and water flow stabilization and to check any leakage. Note that, Figure 2.8 shows the measurements from pressure sensor instrumented in the leg between the high-pressure pump and heat exchanger (Figure 2.4). Figures 2.9 and 2.10 show the corresponding test frame load and position sensor measurements, respectively. From Figure 2.9 it can be seen that due to transient effect of pressurization, the load cell measurement drops to a value of -1150 lbf and as the pressure is stabilized, the load reduced to a stabilized value of -550 lbf. Note that due to stroke control (with zero amplitude stroke set point), the above-mentioned load was not transferred to the specimen, rather just an attribute of load cell measurements. Similar transient and subsequent stabilization in frame position sensor measurements can be seen in Figure 2.10. These types of information are required for accurate processing of the sensor data acquired during fatigue testing. For example, the above-mentioned stabilized value of load cell measurements (i.e., of -550 lbf) should not be considered as preload and should appropriately be removed as an offset from load cell measurements acquired during the fatigue test. In addition, the flow sensor, the conductivity sensor, and thermocouple (TC) readings were also acquired during this stage to ascertain the test conditions. For example, Figures 2.11 and 2.12 show the flow rates and conductivity measurements during this stage of test. Figure 2.13 shows the temperature measurements from all TCs, whereas Fig. 2.14 shows a magnified view showing only the gauge area TC (TC-3, 4 and 5; see Figure 2.5) reading. Figure 2.11 shows a reduced flow rate during 9-20th hour. This could be due to bubbles or cavitation inside the loop.

2.3.2 *Heating up and temperature stabilization of loop*

During this stage, the frame was maintained under load control with zero set point amplitude. Then the temperature of the loop was increased in steps such that the temperature at gauge is to reach ~300°C (~572°F). For the purpose, both the autoclave and preheater temperatures were increased in multiple steps. The heat up was performed over approximately 2-2.5 hours. After

the gage area temperature reached the desired value, the test condition was maintained at that stage for approximately another 20 hours (up to approximately 44th hour from start of the test). The corresponding sensor measurements (from approximately 22nd to 44th hour from the start of the test) can be seen from Figures 2.7 to 2.14. Also, Figure 2.15 shows the LABVIEW screen shot showing TC measurement spatial distribution at ~43.96 h. This shows that, the gage area temperature was stabilized to the desired temperature of 300°C.

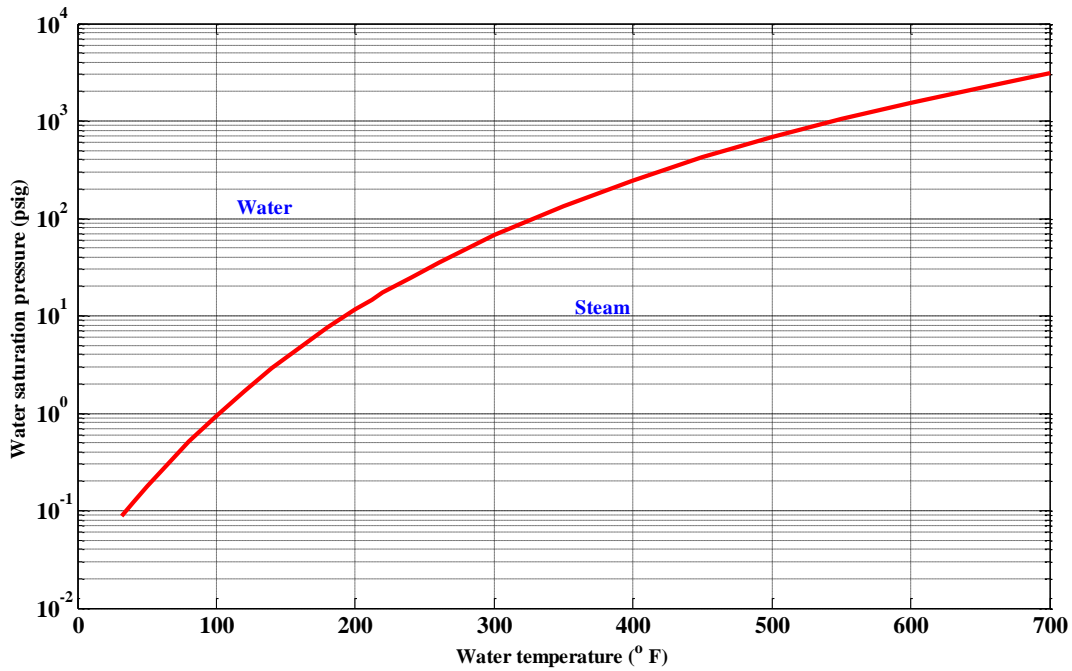


Figure 2.6 Water temperature versus corresponding water saturation pressure

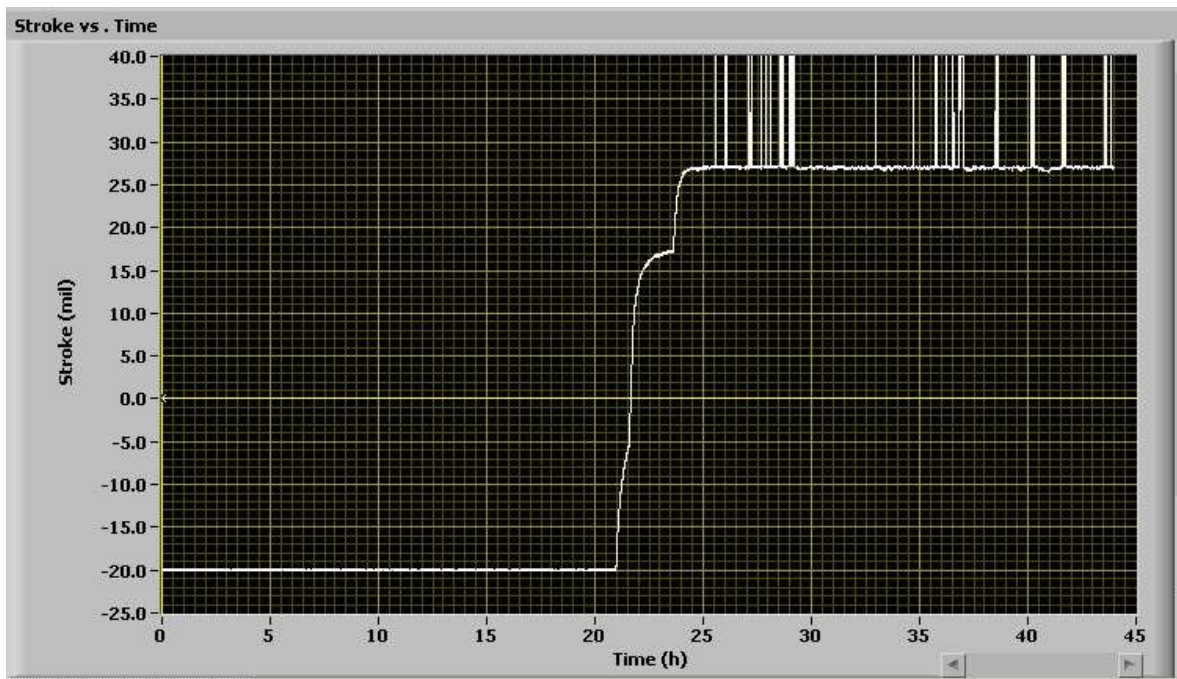


Figure 2. 7 LABVIEW screen shot showing the stroke sensor reading during loop pressurization stage and afterward

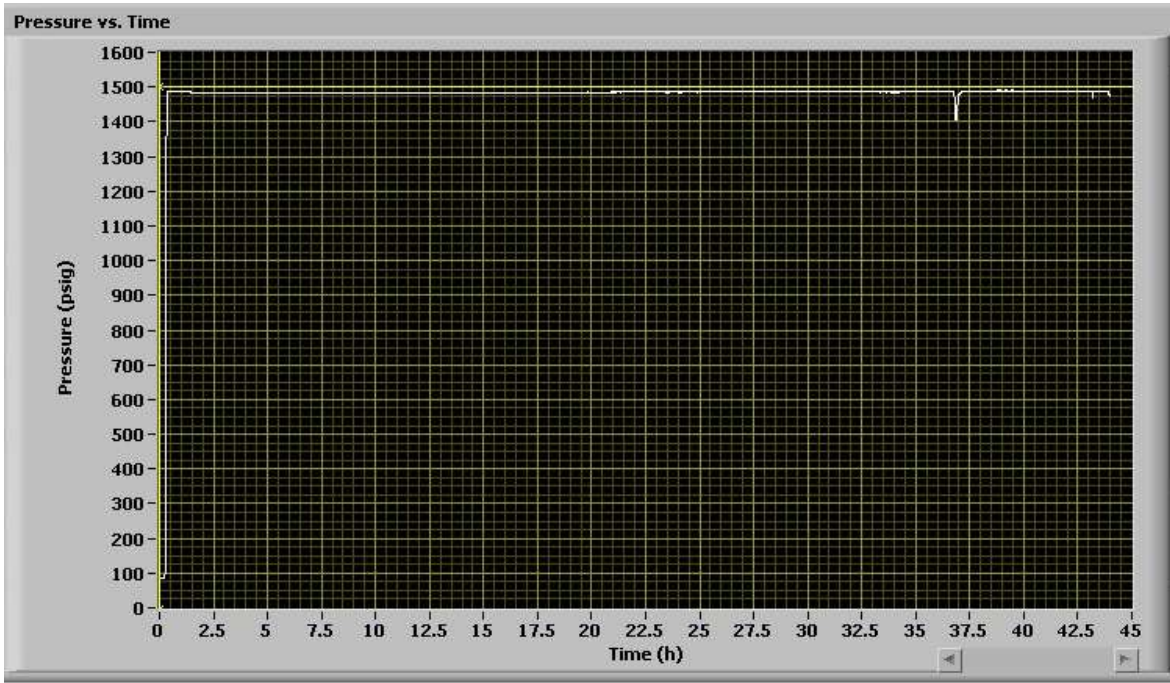


Figure 2. 8 LABVIEW screen shot showing the loop water pressure with respect to time during loop pressurization stage and afterward

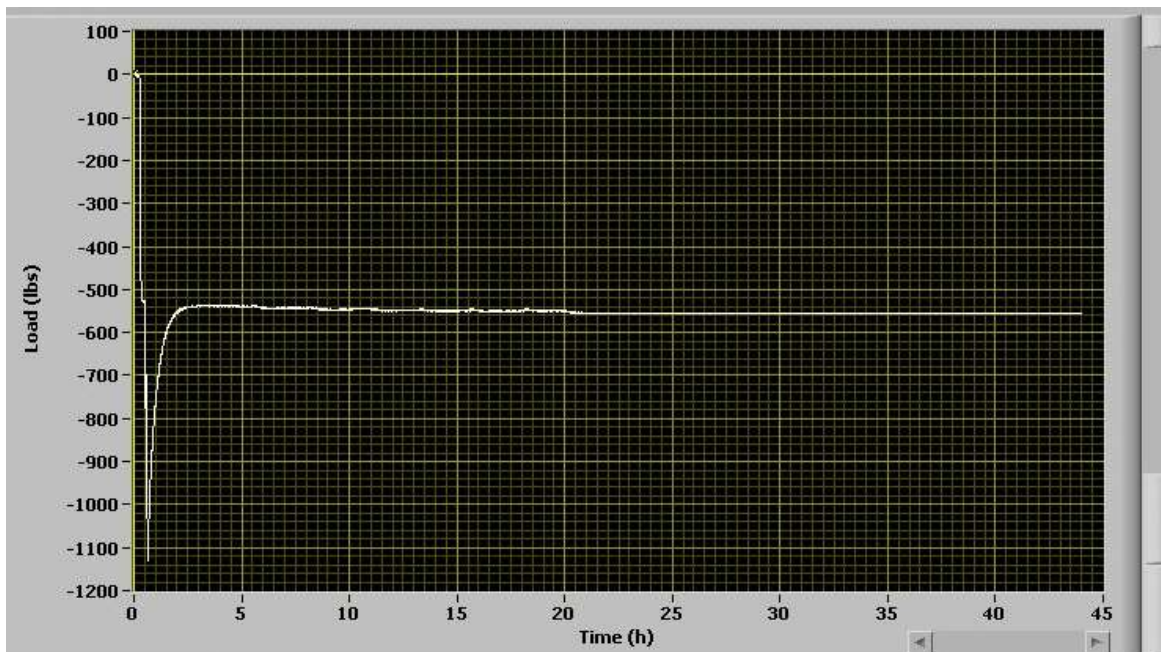


Figure 2. 9 LABVIEW screen shot showing the frame load sensor reading during loop pressurization stage and afterward

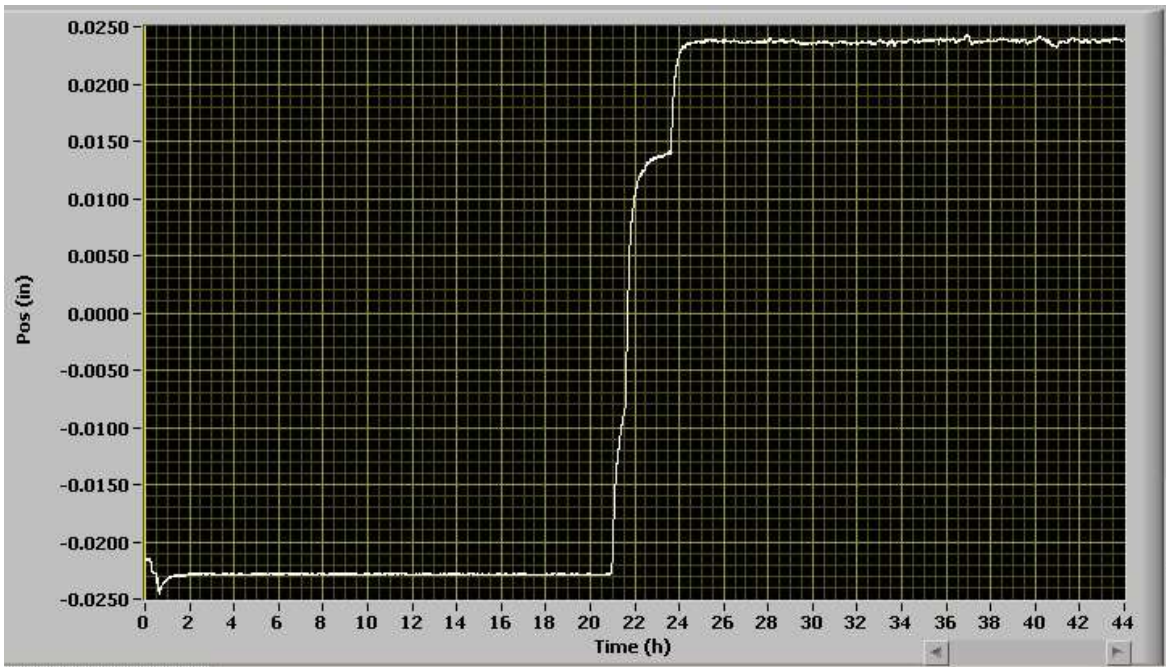


Figure 2. 10 LABVIEW screen shot showing the frame position sensor reading during loop pressurization stage and afterward

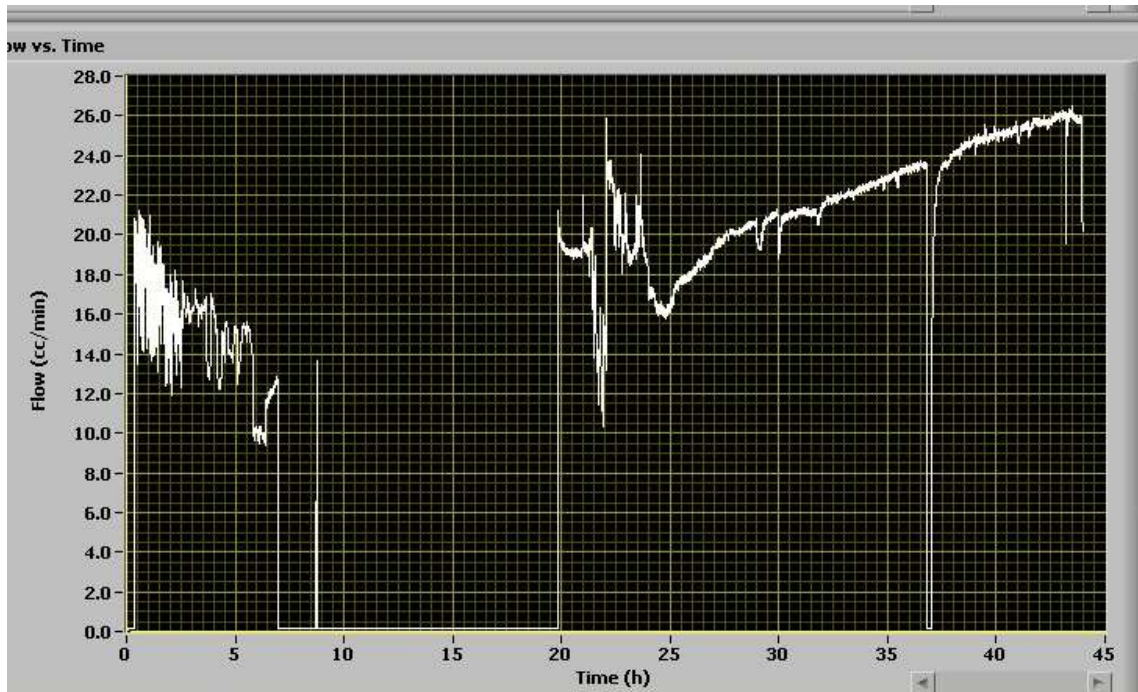


Figure 2. 11 LABVIEW screen shot showing loop flow sensor reading during loop pressurization stage and afterward

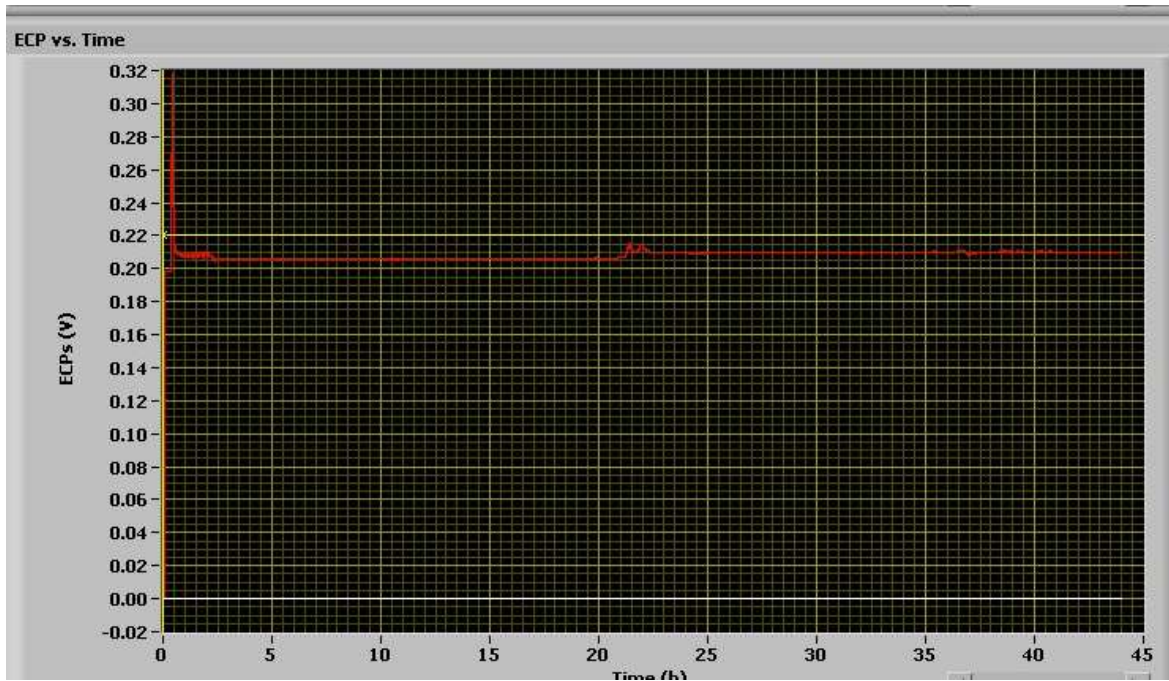


Figure 2. 12 LABVIEW screen shot showing conductivity (measured through ECP sensor channel & with a multiplication factor of $1e-2$) sensor reading during loop pressurization stage and afterward

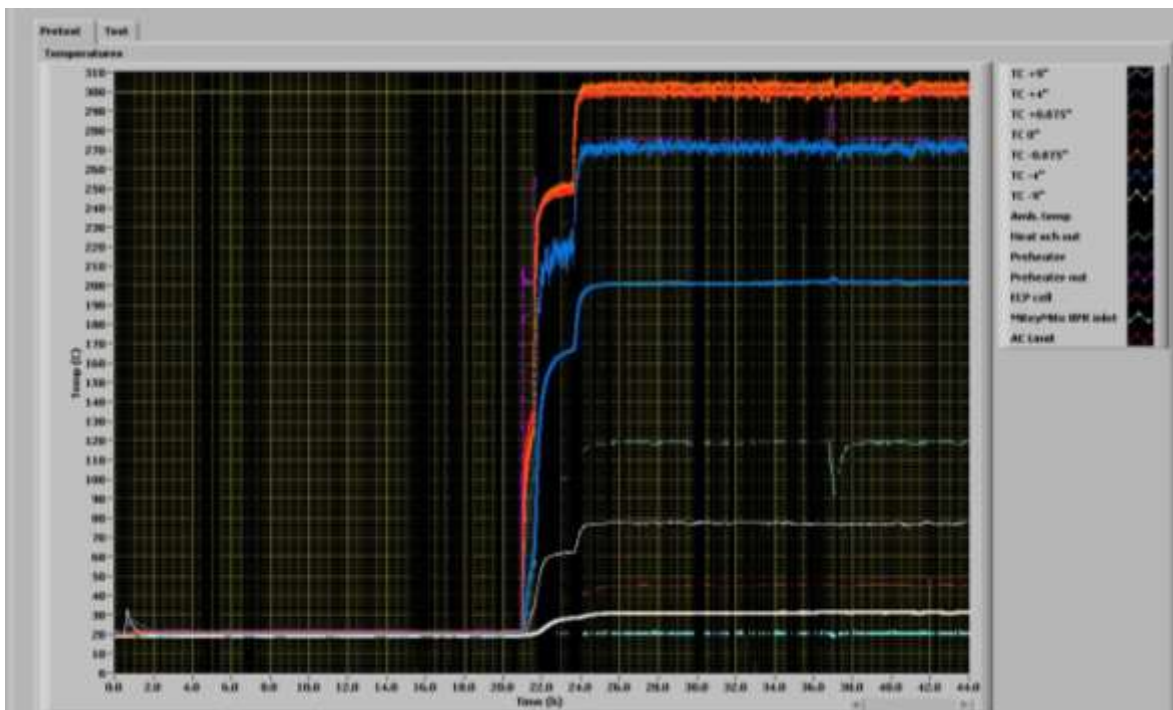


Figure 2. 13 LABVIEW screen shot showing TC (from all TC) reading during loop pressurization stage and afterward

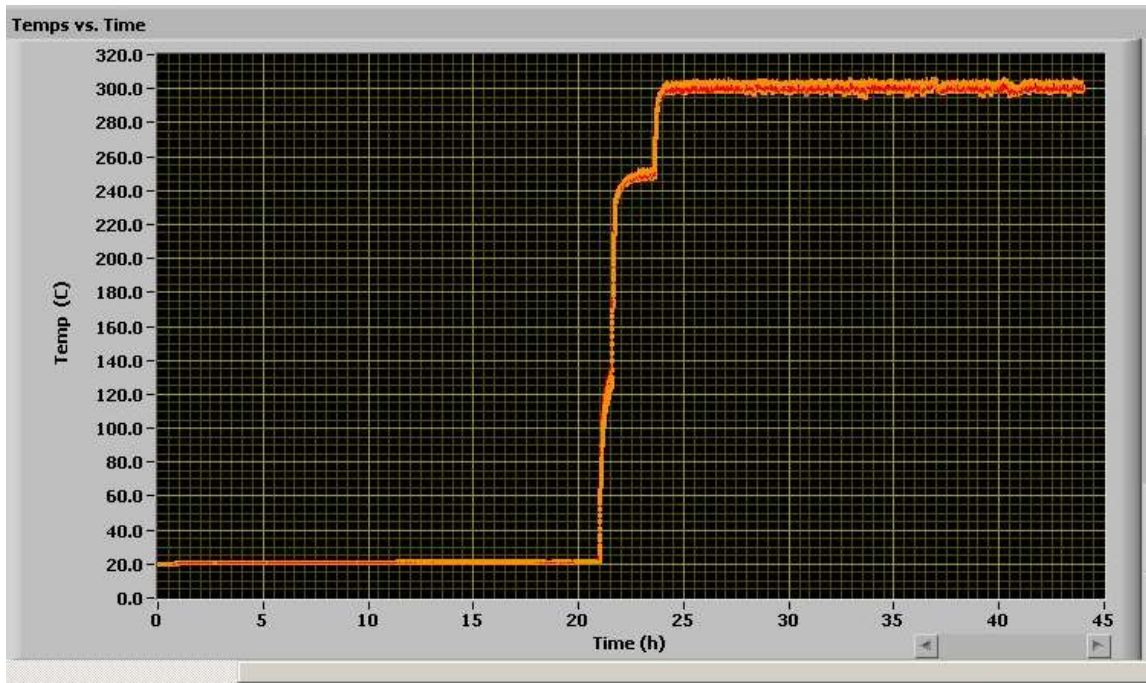


Figure 2. 14 LABVIEW screen shot showing TC (in gauge area) reading during loop pressurization stage and afterward

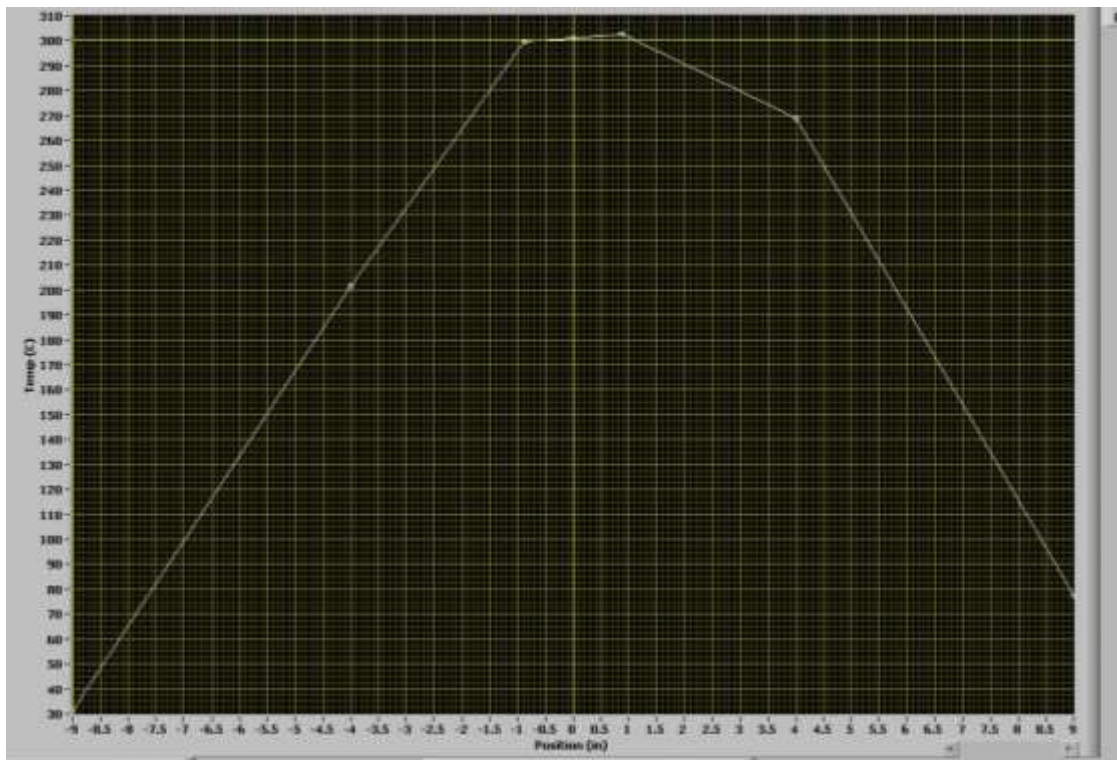


Figure 2. 15 LABVIEW screen shot showing TC measurement spatial distribution approximately at 43.96 h

2.3.3 Fatigue test under stroke control

After the temperature was stabilized, the control mode was switched to stroke mode and the fatigue test was conducted. The stroke input was chosen such that the gauge area strain amplitude can be maintained at 0.5%. The time period of each cycle was maintained at 20 seconds. This was to achieve an equivalent strain rate of $0.1\% \text{ s}^{-1}$. The corresponding stroke amplitude of 5.1693 mil was selected, based on a stroke-strain mapping relation. For this purpose, the 316SS elevated temperature (300°C), $0.1\% \text{ s}^{-1}$ strain rate tensile test (T04) data such as frame crosshead stroke and gauge area strain (extensometer) measurements were used to map a relation between stroke and strain. This was achieved by fitting the stroke and strain data using a 7th order polynomial given below:

$$\varepsilon = a_0 + a_1d_s + a_2d_s^2 + a_3d_s^3 + a_4d_s^4 + a_5d_s^5 + a_6d_s^6 + a_7d_s^7 \quad 2.1$$

with $a_{i=0,1,2,3,4,5,6,7} = -0.0021055, 2.3843, -74.608, 1704, -12834, 46379, -81825$ and 56605 , respectively. In Eq. 2.1 ε and d_s represent strain (in %) and stroke displacement (in mm), respectively. Figure 2.16 shows the original and regenerated stroke versus strain curve using the above mentioned polynomial function. For environmental test since the test specimen would be inside the autoclave and it will not be possible to measure gauge area displacement (using an extensometer), the above mentioned polynomial equation was used to estimate the corresponding

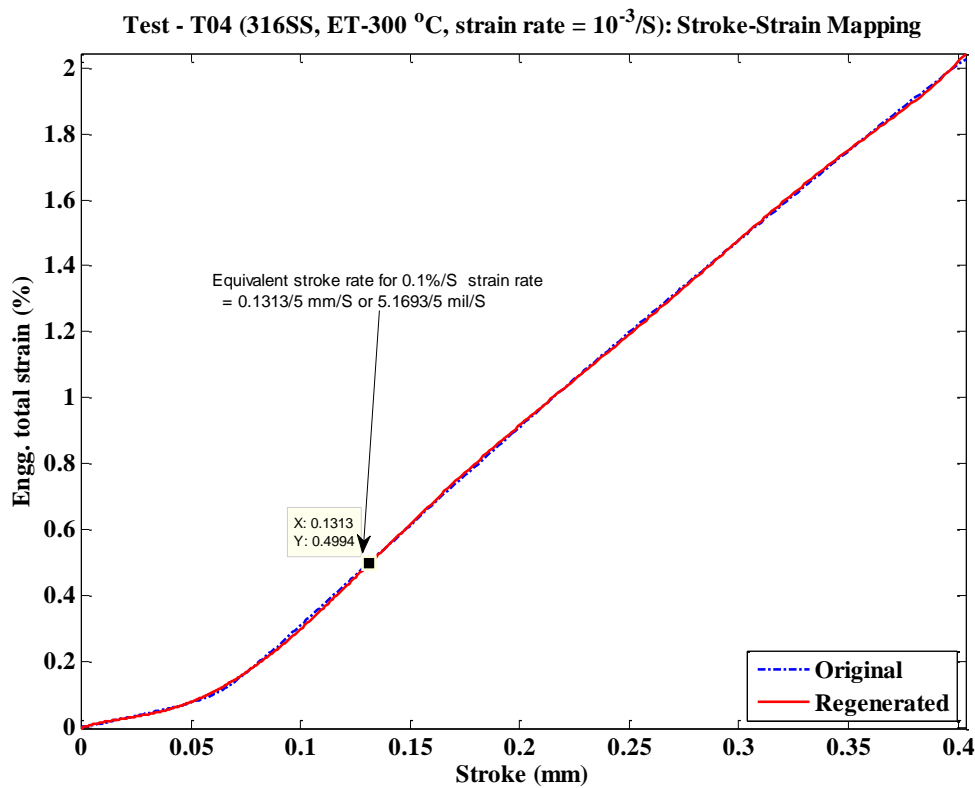


Figure 2. 16 Stroke strain mapping based on in-air but elevated temperature (300°C) tensile test data for 316SS specimen

strain for the measured stroke in environmental fatigue tests. Note that both the in-air test frame (Test frame 5) and environmental test frame (Test frame 9) are similar in set up (e.g., load cell, frame actuator, pull rod, etc.) and it is expected that, both will have similar overall compliance and the above estimated polynomial function based on in-air test frame data is also applicable for the test conducted using environmental test frame. However, the test conditions (e.g., similar geometry of 316SS specimen and test temperature 300°C) other than the water environment in environmental test cases should be remain same as in the in-air test condition of T04 tensile test. In PWR water and high purity water environments, it is assumed that the tensile test properties (stress, strain, etc.) will not change much compared to the corresponding in-air tensile test condition.

During this stroke control fatigue test the LABVIEW program was reset to collect data with zero starting time. During this stage, the fatigue test related measurements (e.g. load, stroke, displacement) and loop condition related measurements (e.g. temperature, pressure, flow rate and conductivity) were taken. The fatigue test related measurements were further processed for material parameter estimation and will be presented in next section. However, the LABVIEW snap shot of the field condition related measurements are presented in Figs 2.17 to 2.22.

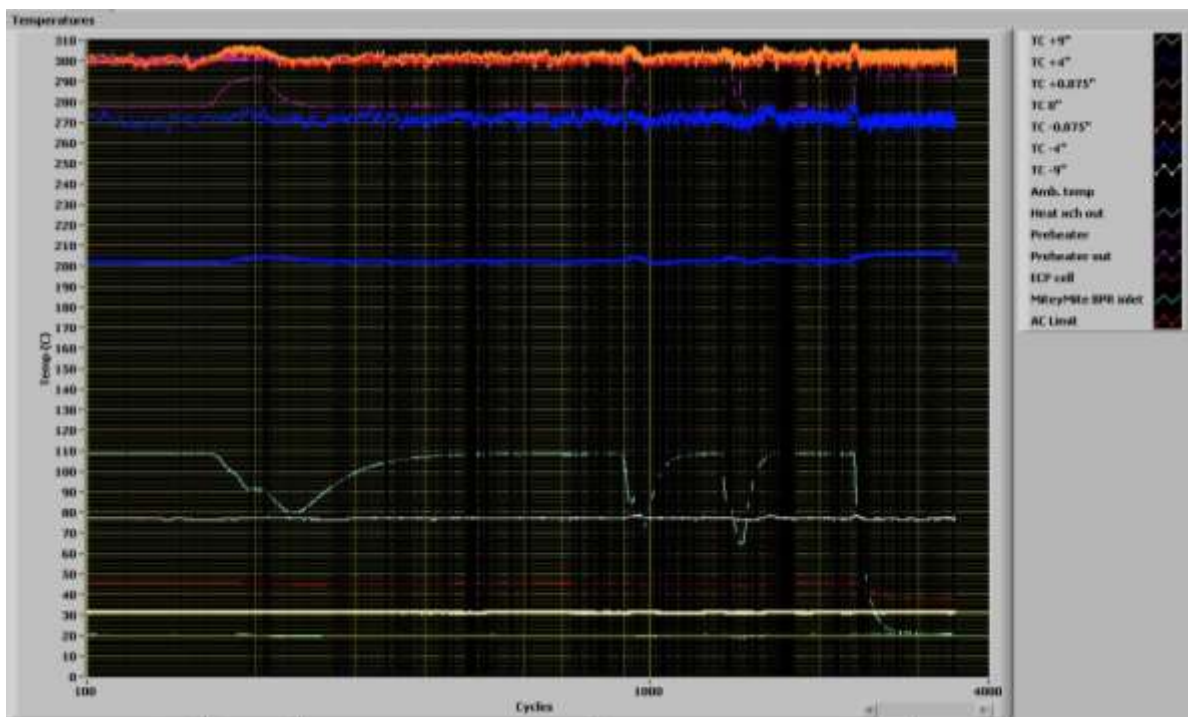


Figure 2. 17 LABVIEW screen shot (at the end of test with 3480 fatigue cycle) showing TC (from all TC) reading during main fatigue test

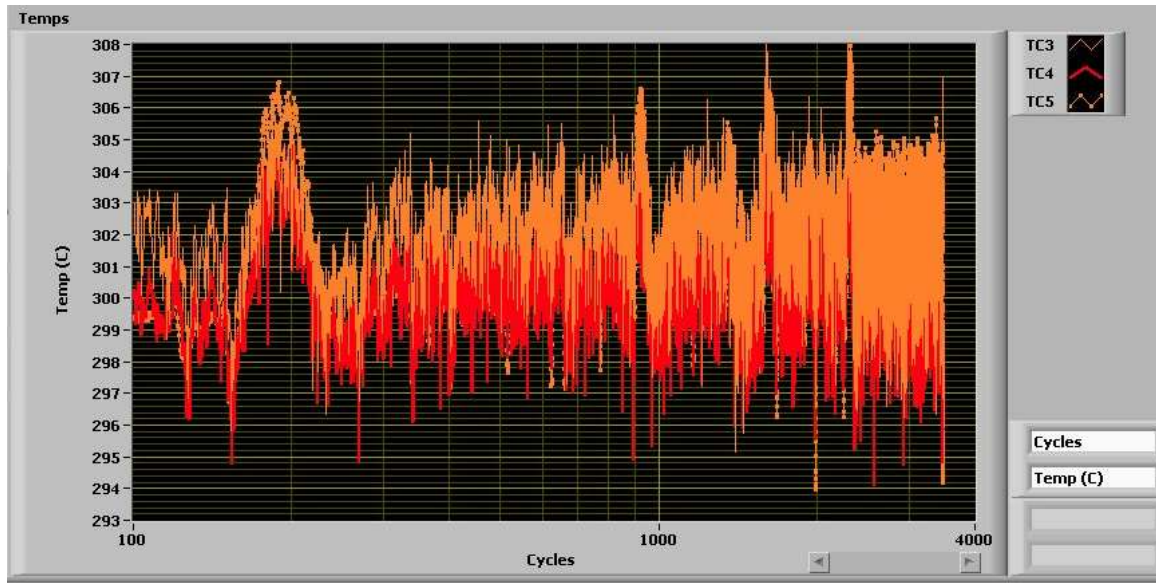


Figure 2. 18 LABVIEW screen shot (at the end of test with 3480 fatigue cycle) showing TC (from gauge area TC-3, 4 and 5) reading during main fatigue test

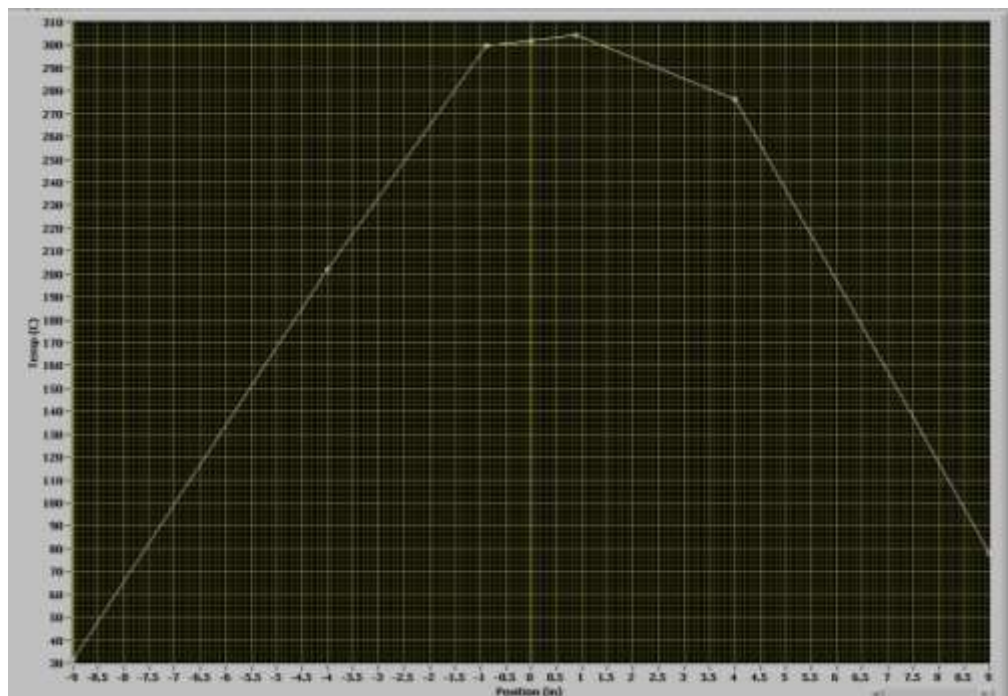


Figure 2. 19 LABVIEW screen shot showing TC measurement spatial distribution approximately at the end of test with 3480 fatigue cycle



Figure 2. 20 LABVIEW screen shot (at the end of test with 3480 fatigue cycle) showing the loop water pressure with respect to fatigue cycles during main fatigue test

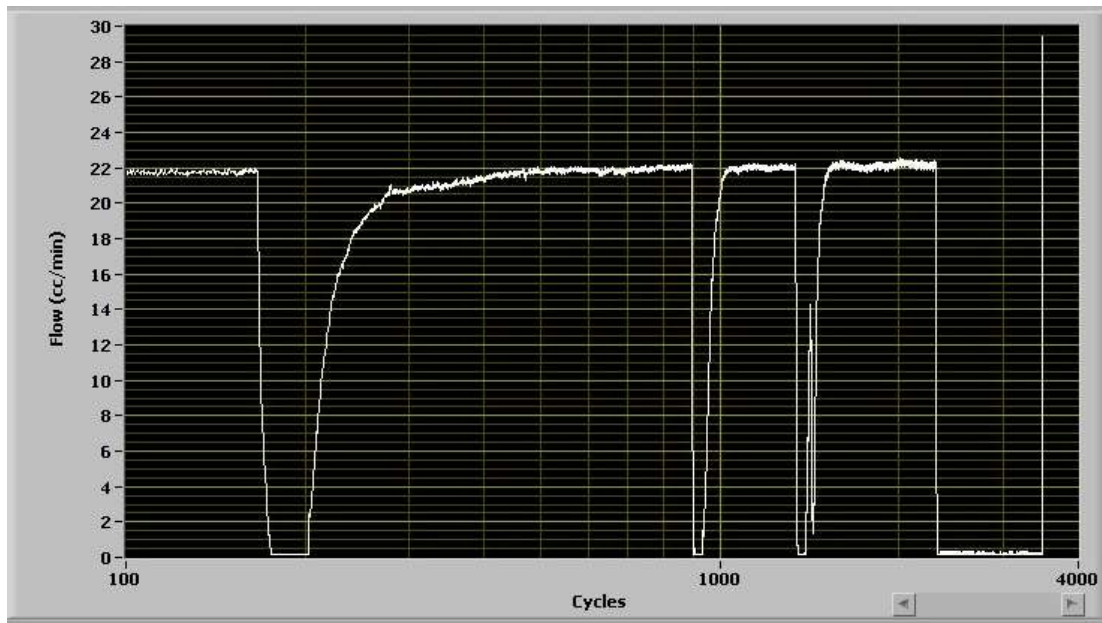


Figure 2. 21 LABVIEW screen shot (at the end of test with 3480 fatigue cycle) showing the loop water flow rate with respect to fatigue cycles during main fatigue test

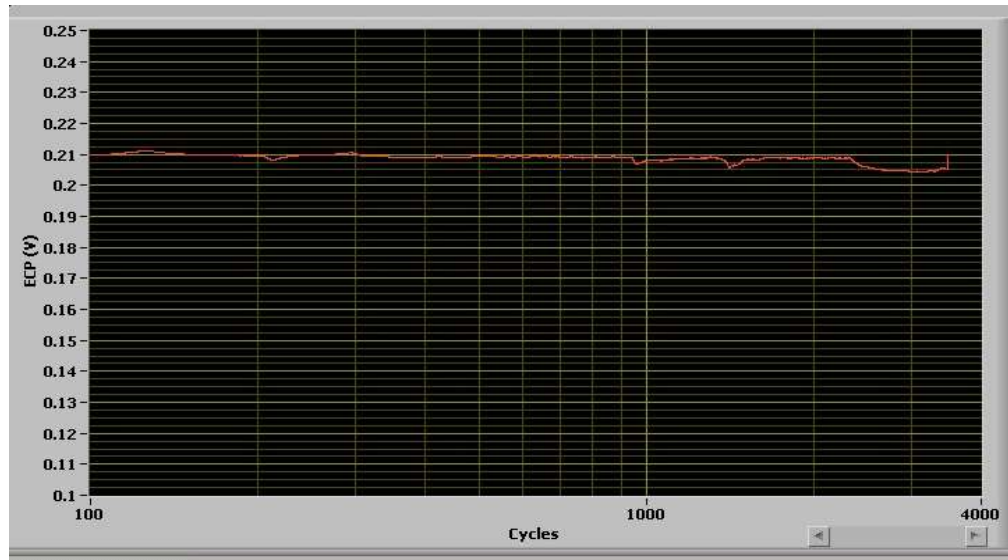


Figure 2. 22 LABVIEW screen shot (at the end of test with 3480 fatigue cycles) showing the loop water conductivity (measured through ECP sensor channel & with a multiplication factor of $1e-2$) with respect to fatigue cycles during main fatigue test

2.4 F14 Fatigue Test Data Processing & Material Characterization Results

The F14 environmental fatigue test data are processed and modeled to estimate material parameters of 316SS under PWR environment. It is assumed that, this data directly can be used for component level fatigue evaluation using commercial finite element code such as ABAQUS. The details of the results are summarized in the following subsections.

2.4.1 Time history of stress, stroke, position and strain

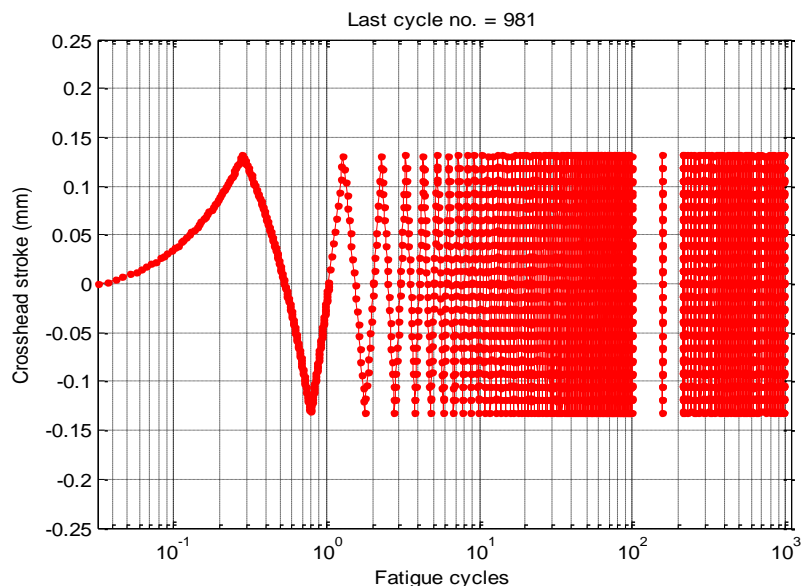


Figure 2. 23 Stroke sensor measurements time history up to first 981 fatigue cycles

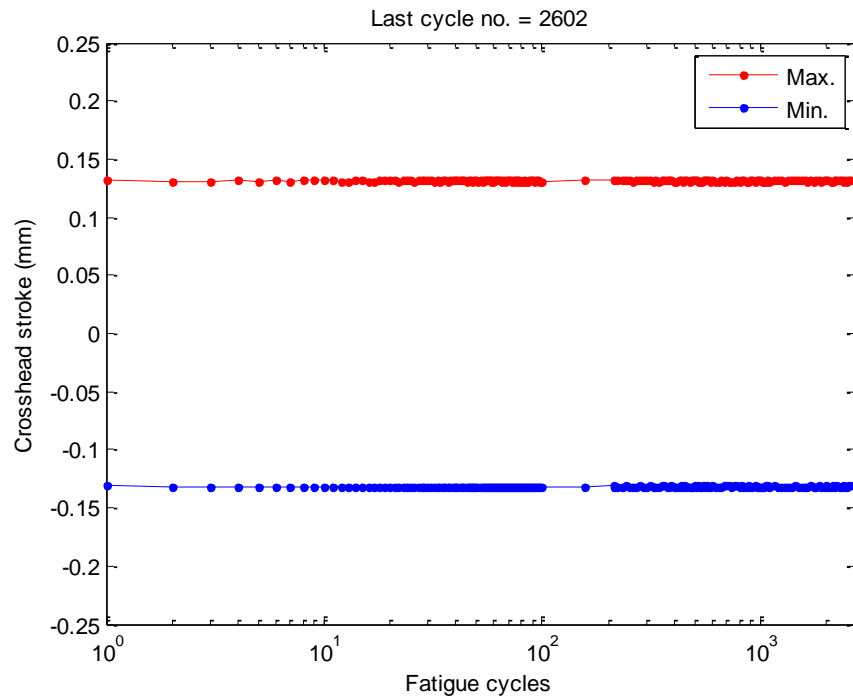


Figure 2.24 Maximum/minimum stroke amplitude up to 25% load drop (2602 cycles)

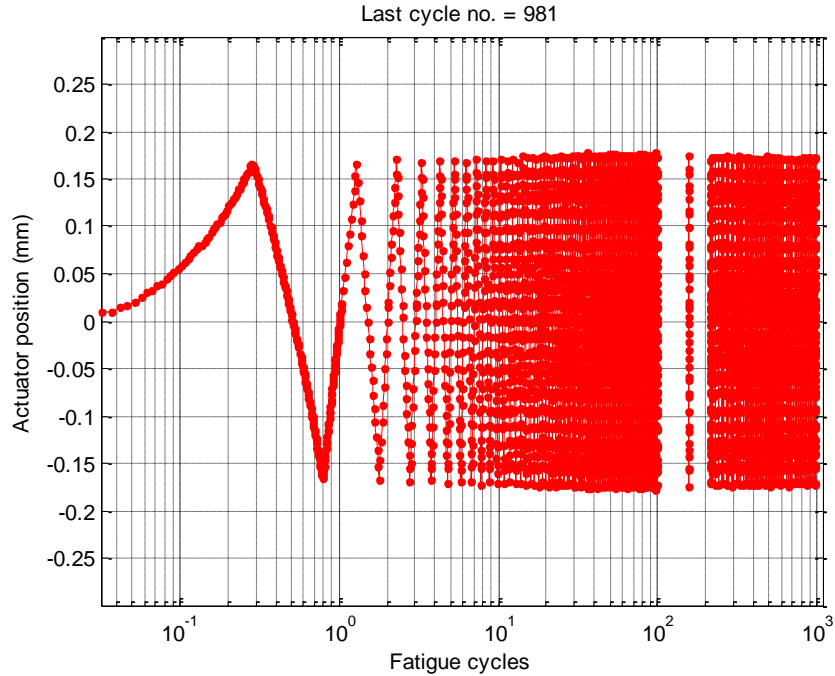


Figure 2.25 Frame position sensor measurements time history up to first 981 fatigue cycles

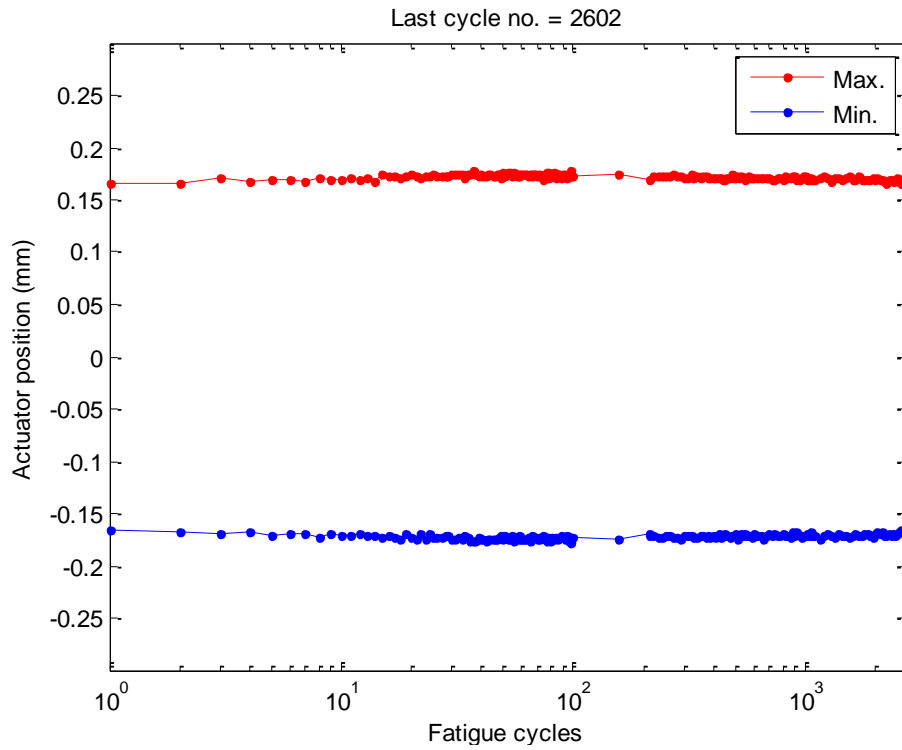


Figure 2. 26 Maximum/minimum actuator position up to 25% load drop (2602 cycles)

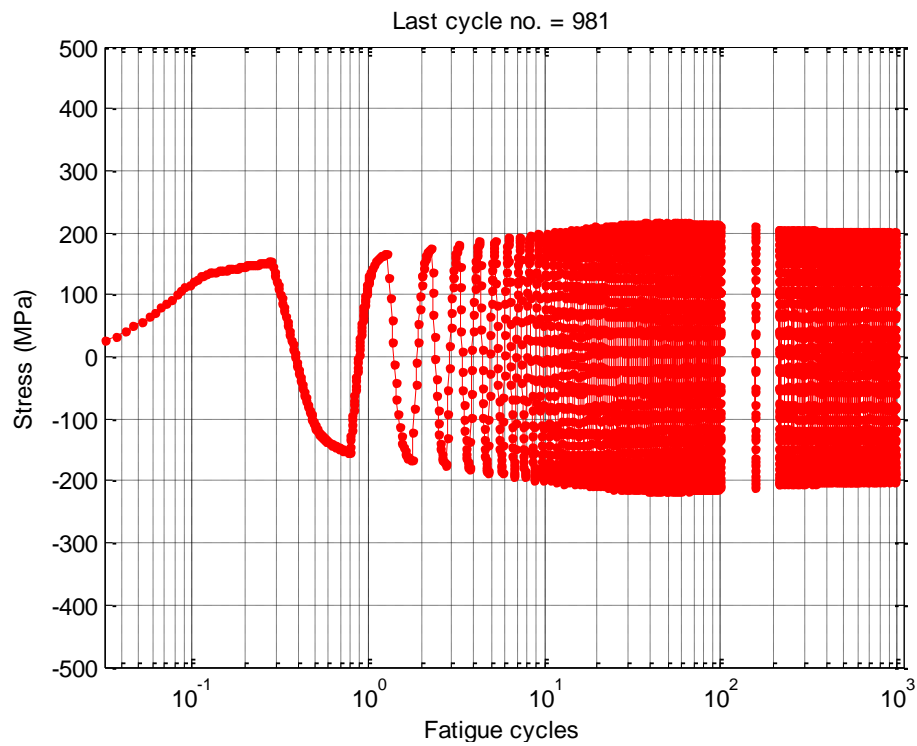


Figure 2. 27 Frame load cell measurements (stress) time history up to first 981 fatigue cycles

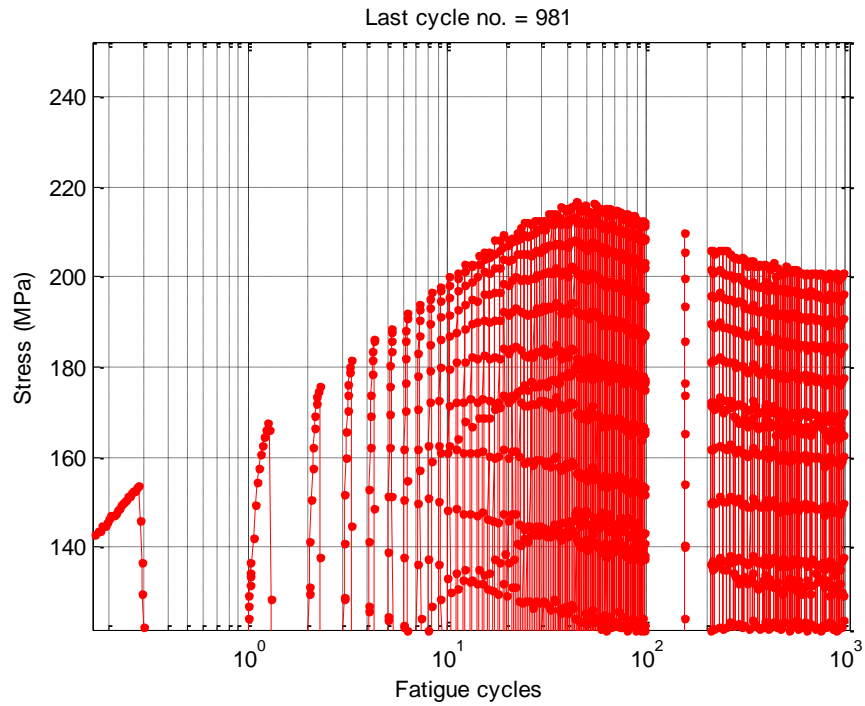


Figure 2. 28 Magnified view of stress history showing stress hardening and softening

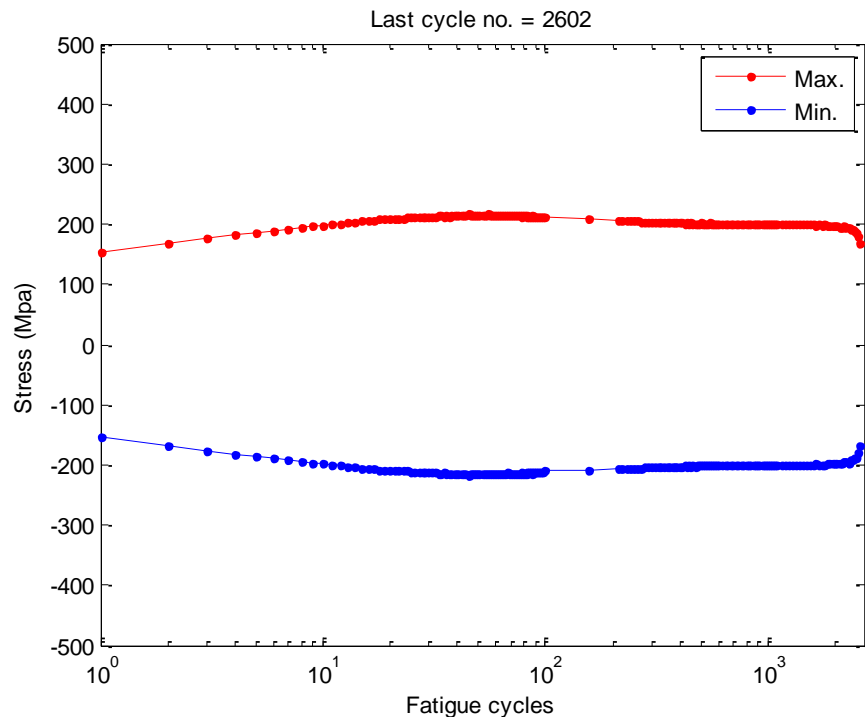


Figure 2. 29 Maximum/minimum stress up to 25% load drop (approx. 2602 cycles)

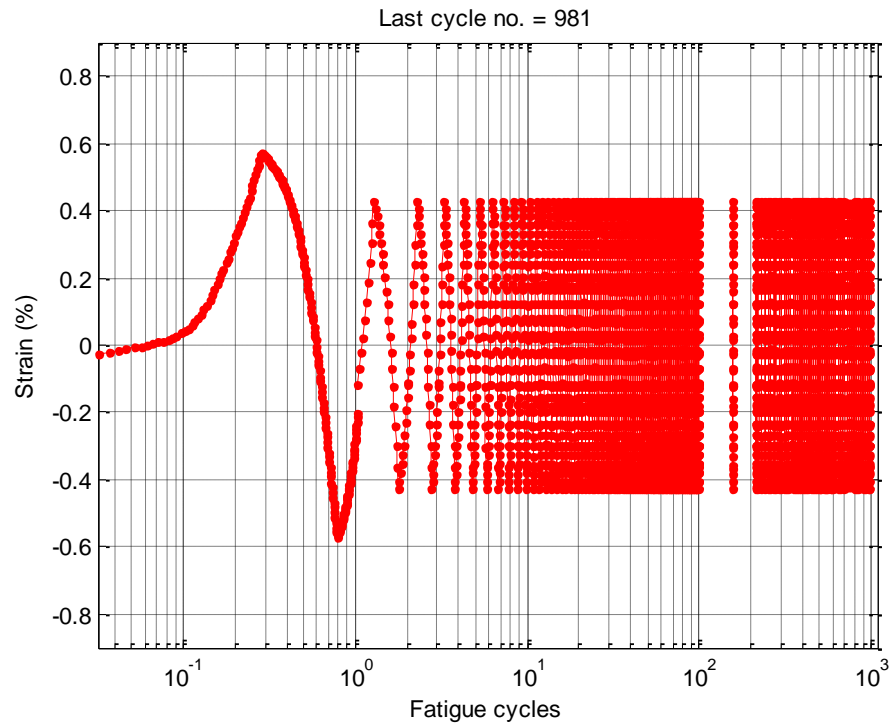


Figure 2. 30 Predicted strain time history up to first 981 fatigue cycles

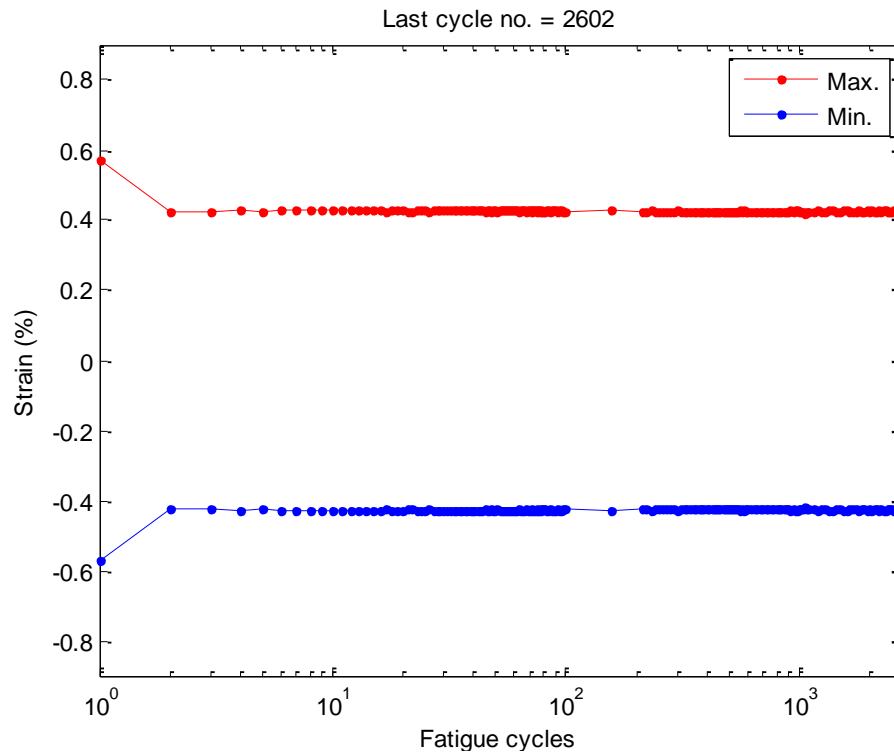


Figure 2. 31 Maximum/minimum strain up to 25% load drop (2602 cycles)

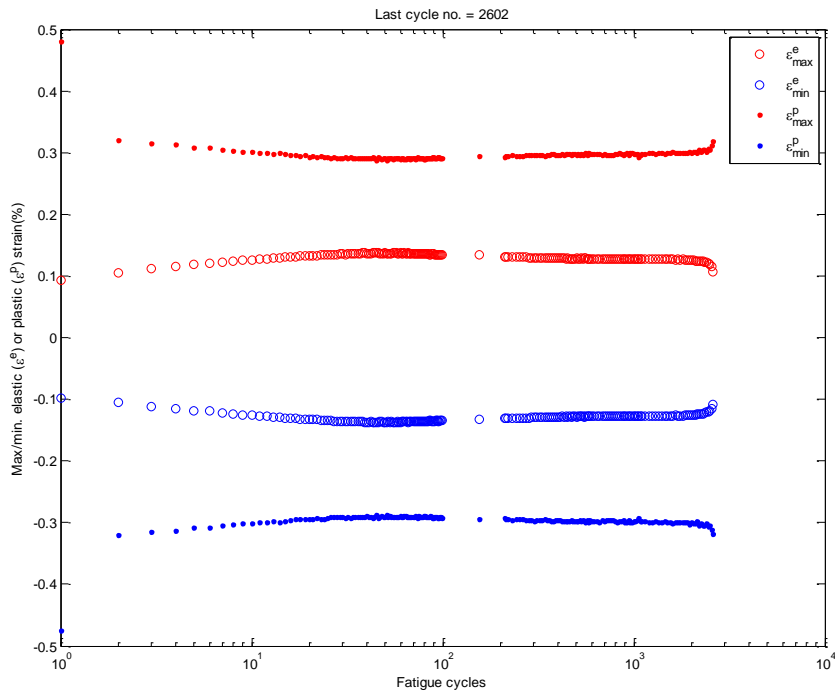


Figure 2. 32 Maximum/minimum elastic/plastic strain up to 25% load drop (2602 cycles)

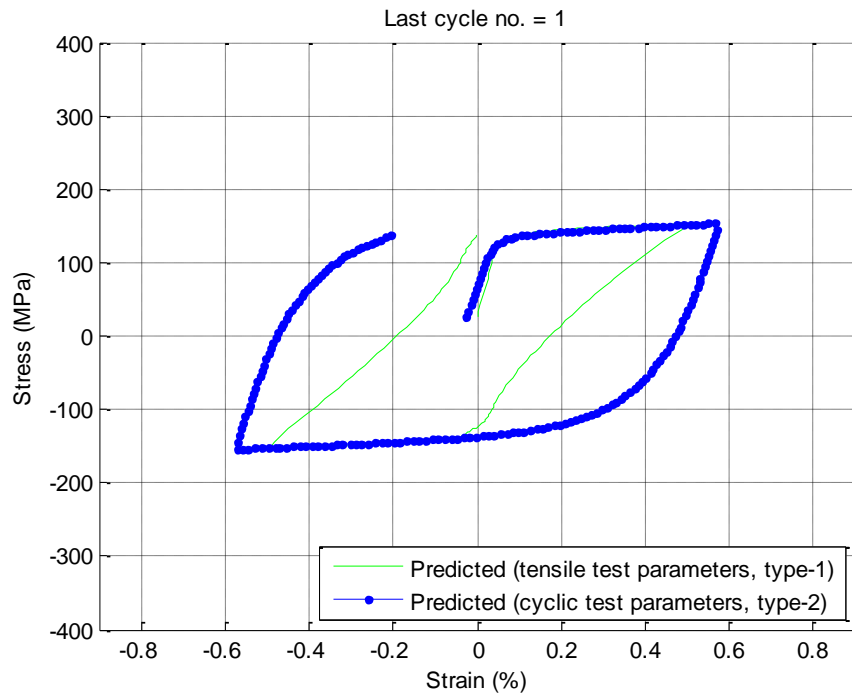


Figure 2. 33 Example of heresies loop (at cycle 1) based on predicted strain using tensile (T04 at 300°C) & cycle test (F13 stroke control, 300°C) parameters

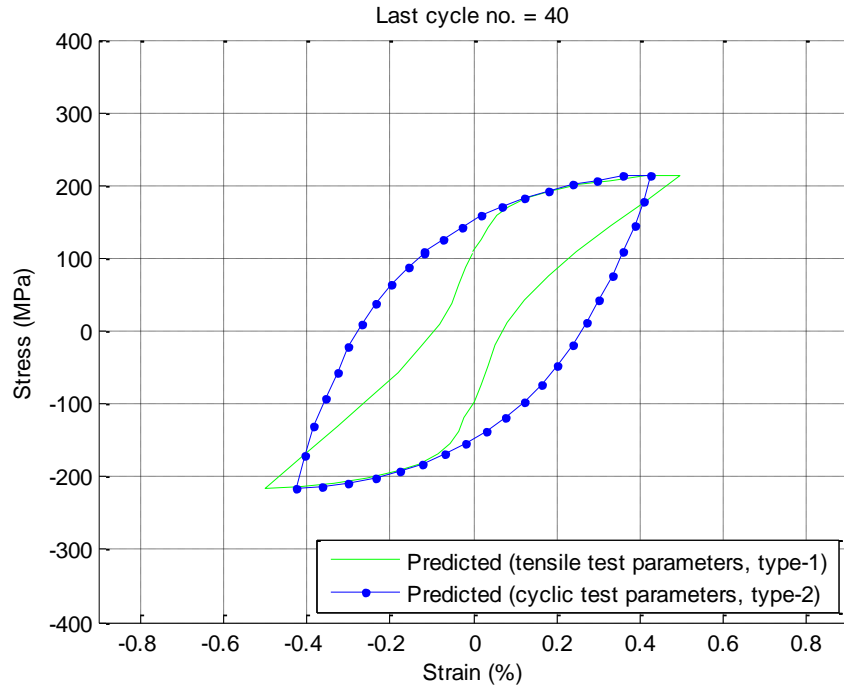


Figure 2. 34 Example of heresies loop (at cycle 40) based on predicted strain using tensile (T04 at 300°C) & cycle test (F13 stroke control, 300°C) parameters

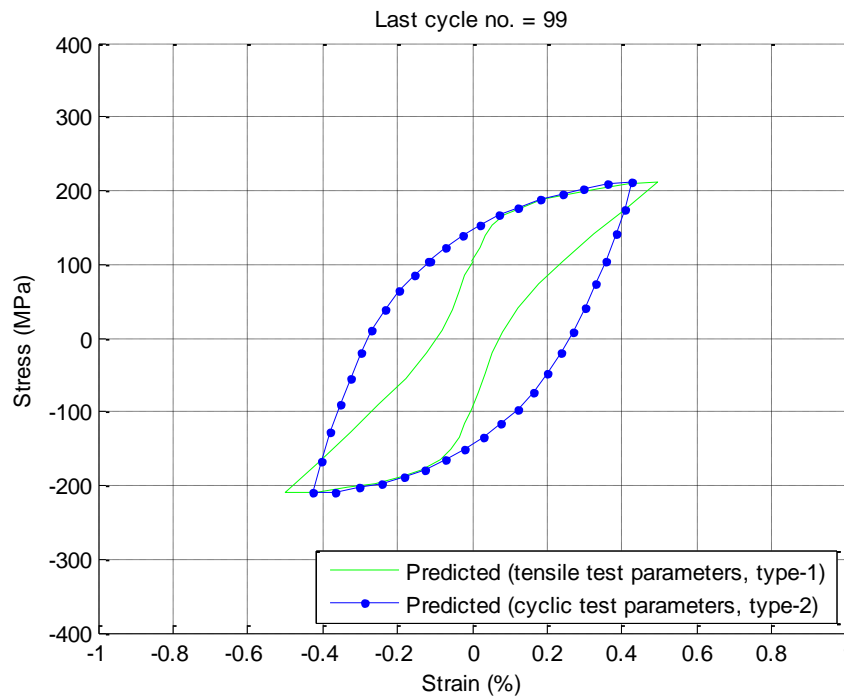


Figure 2. 35 Example of heresies loop (at cycle 99) based on predicted strain using tensile (T04 at 300°C) & cycle test (F13 stroke control, 300°C) parameters

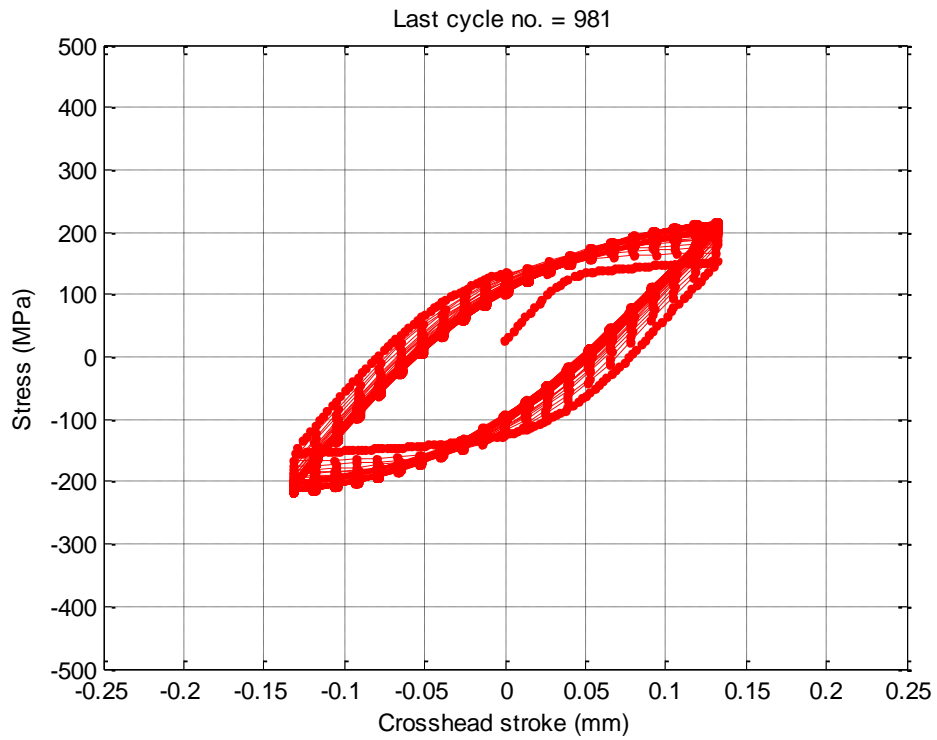


Figure 2. 36 Measured stroke versus stress hysteresis loop up to first 981 fatigue cycle

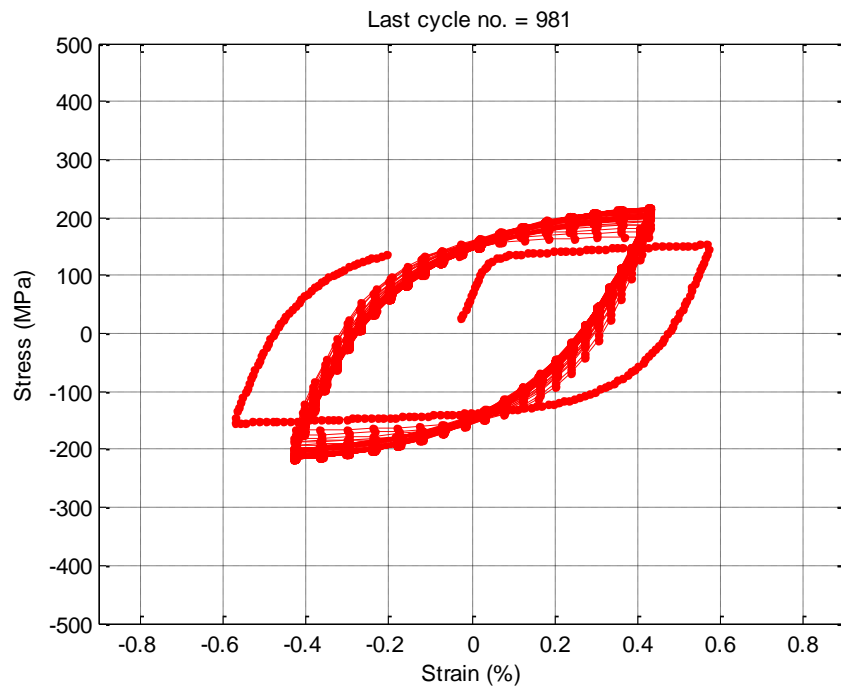


Figure 2. 37 Predicted strain versus stress hysteresis loop up to first 981 fatigue cycle

2.4.2 Evolution of elastic modulus, elastic limit stress, yield stress and accumulated plastic strain

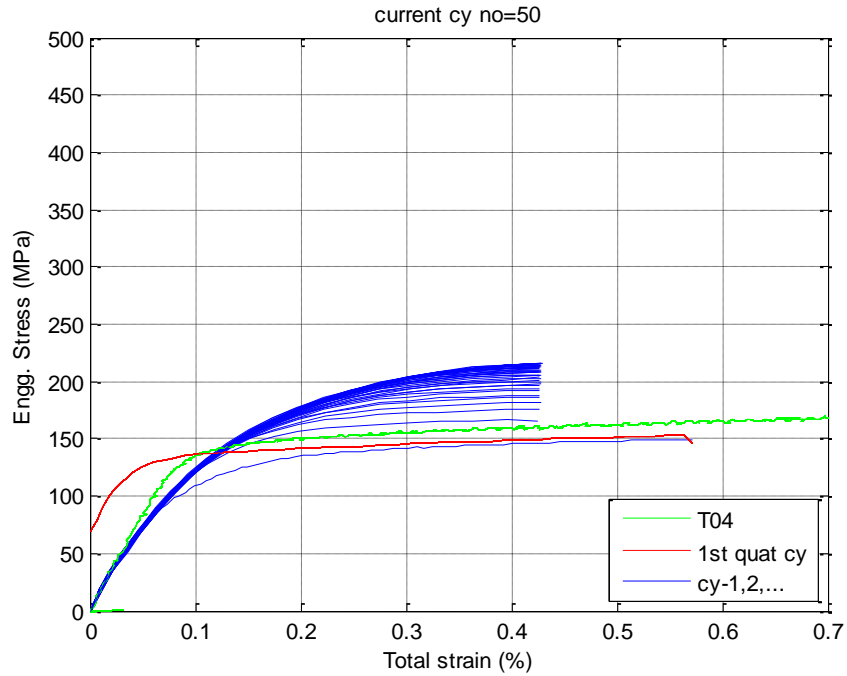


Figure 2.38 Equivalent quarter cycle predicted strain versus measured stress for estimation of evolutionary material parameters

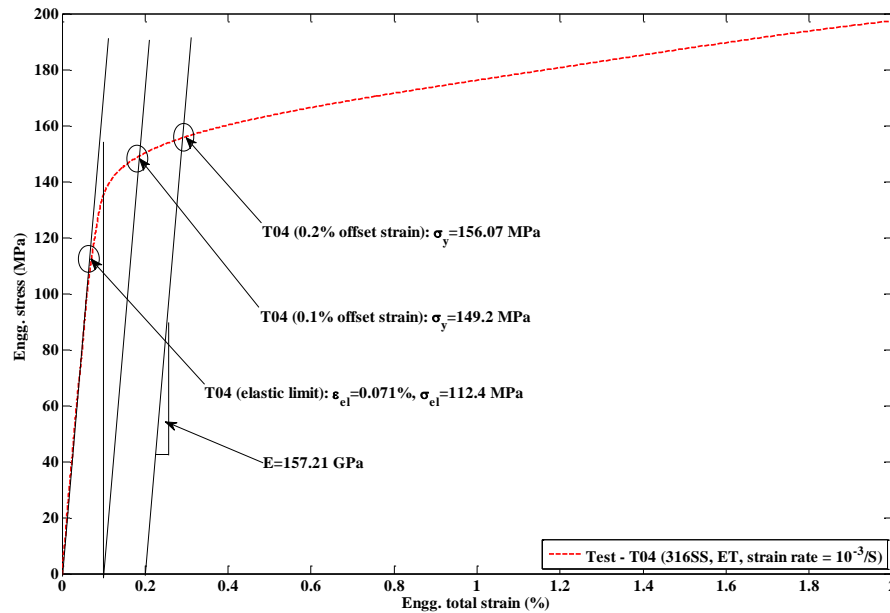


Figure 2.39 Elevated temperature 300°C tensile test (T04) stress-strain curve showing various elastic and yield limits used as reference in F14 material parameter estimation

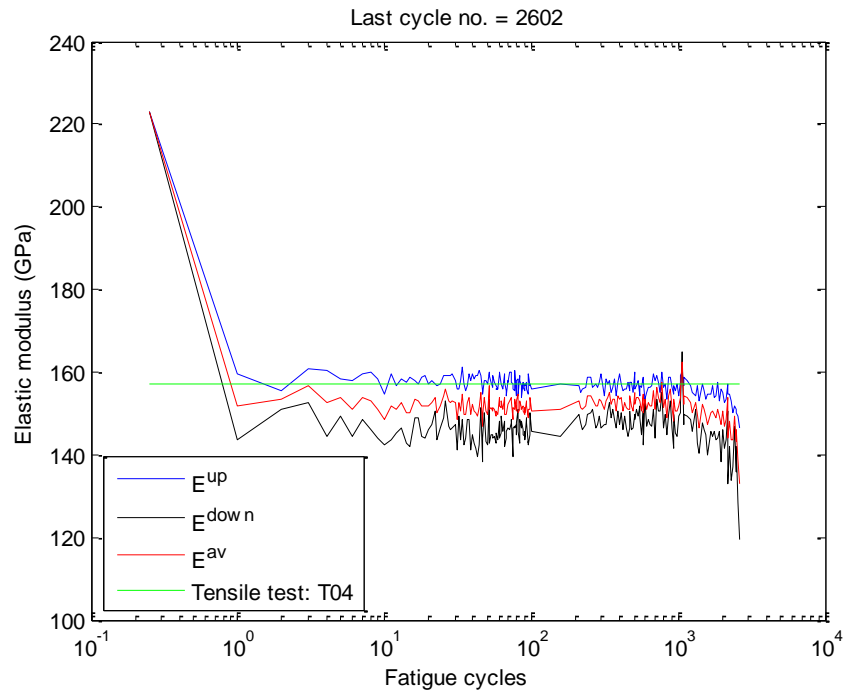


Figure 2. 40 Evolution of elastic modulus for 316SS under PWR condition (as estimated using F14 fatigue test data)

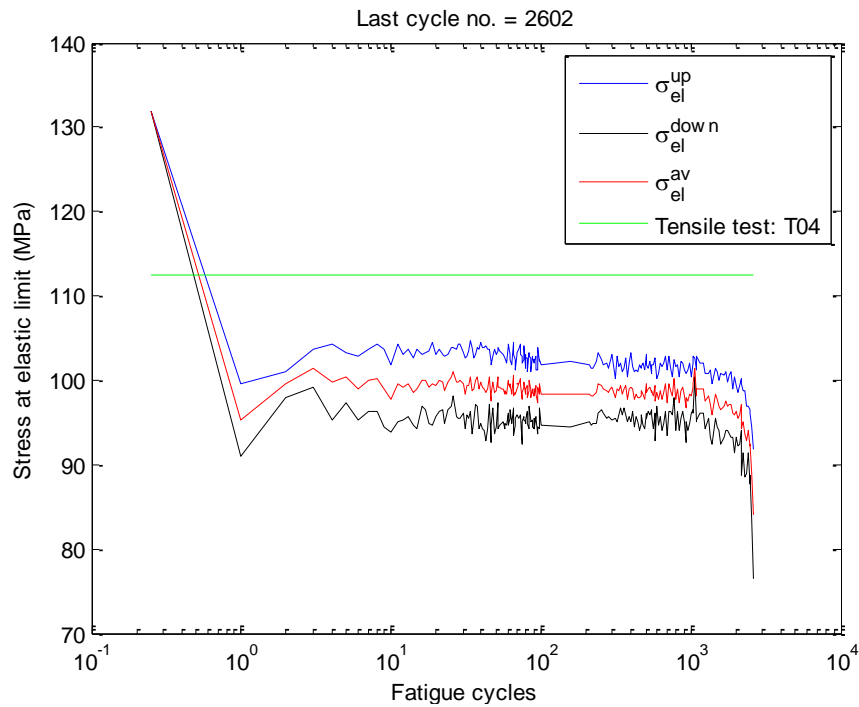


Figure 2. 41 Evolution of elastic limit stress for 316SS under PWR condition

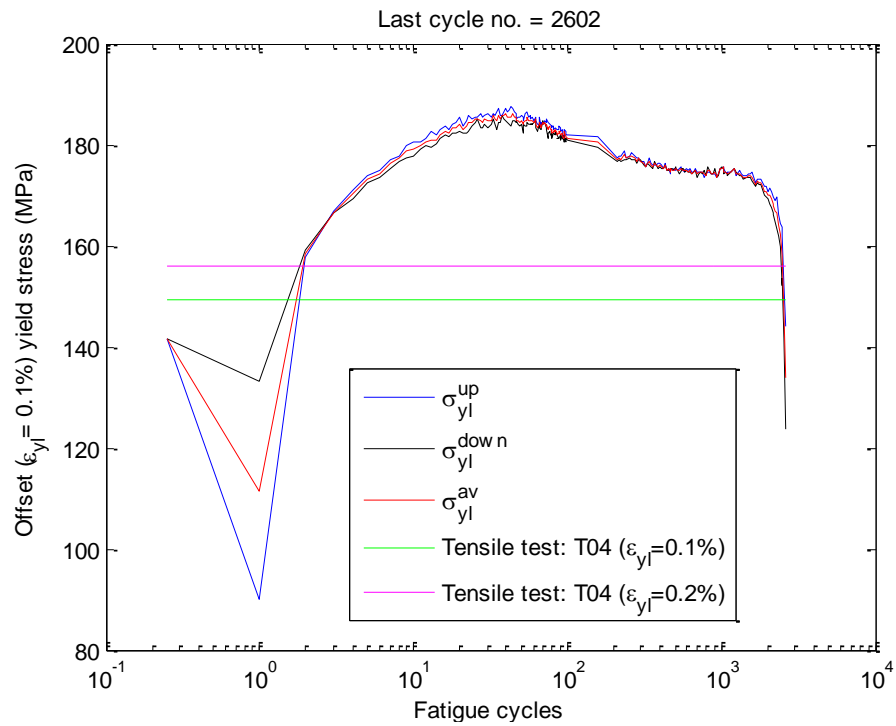


Figure 2. 42 Evolution of 0.1% offset yield stress for 316SS under PWR condition

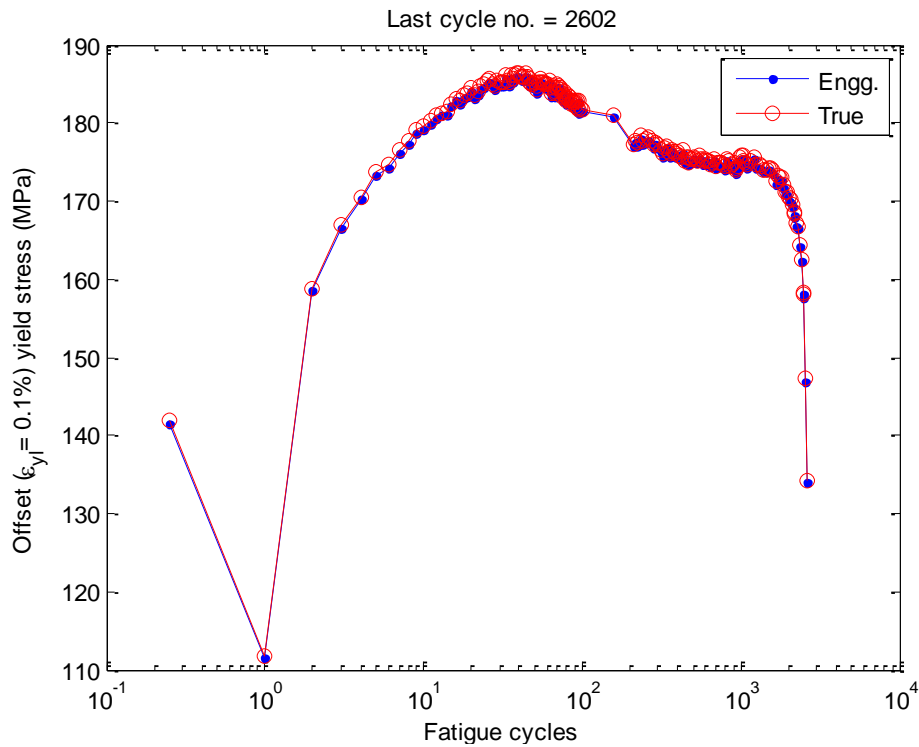


Figure 2. 43 Evolution of engineering versus true average yield stress (note: true yield stress was used to predict hardening/softening parameters)

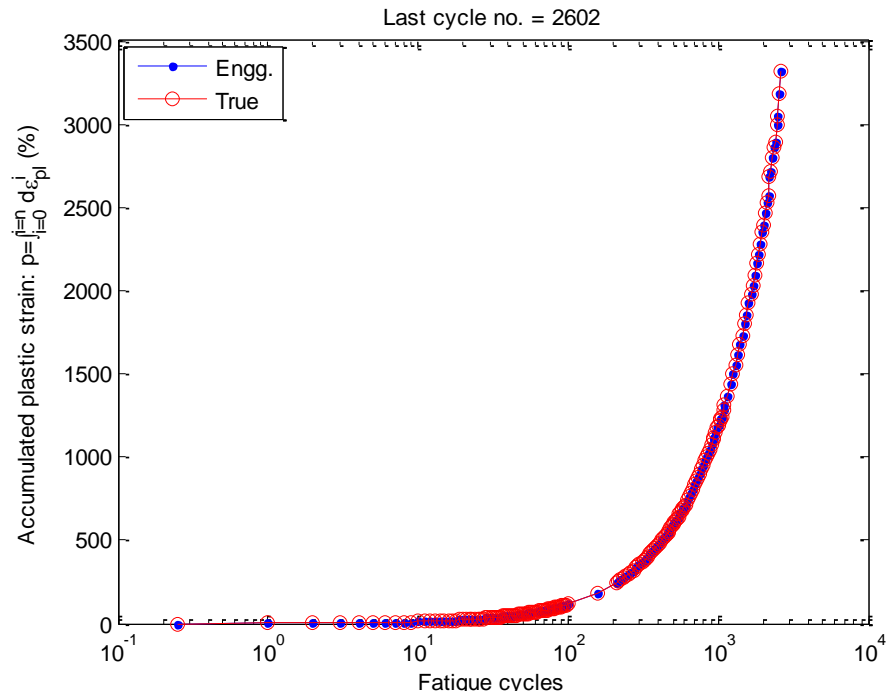


Figure 2. 44 Evolution of engineering versus true accumulated plastic strain (true plastic stress was used to predict hardening/softening parameters)

2.4.3 Evolution of isotropic hardening stress and estimation of isotropic hardening parameters

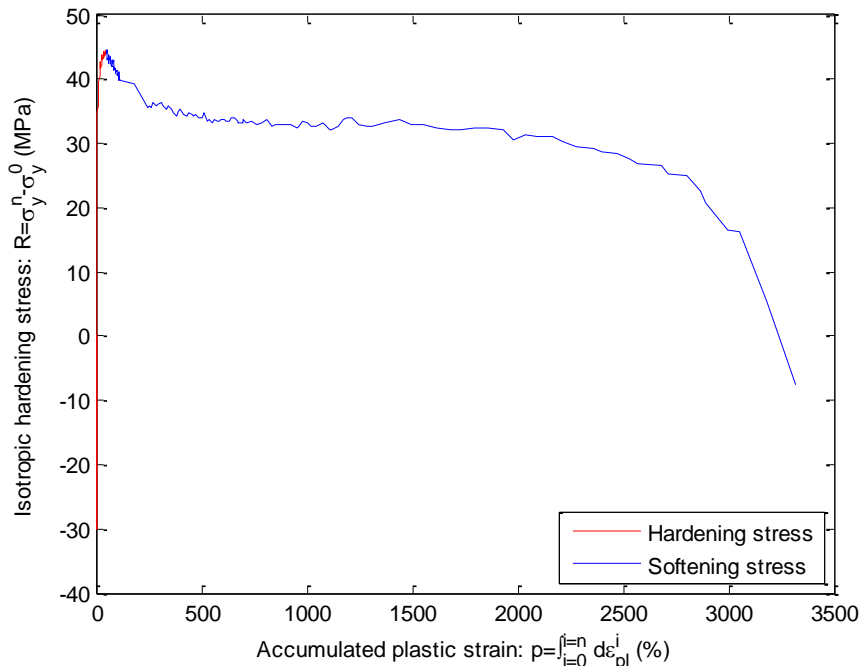


Figure 2. 45 Evolution of isotropic hardening stress up to 25% load drop (2602 cycles)

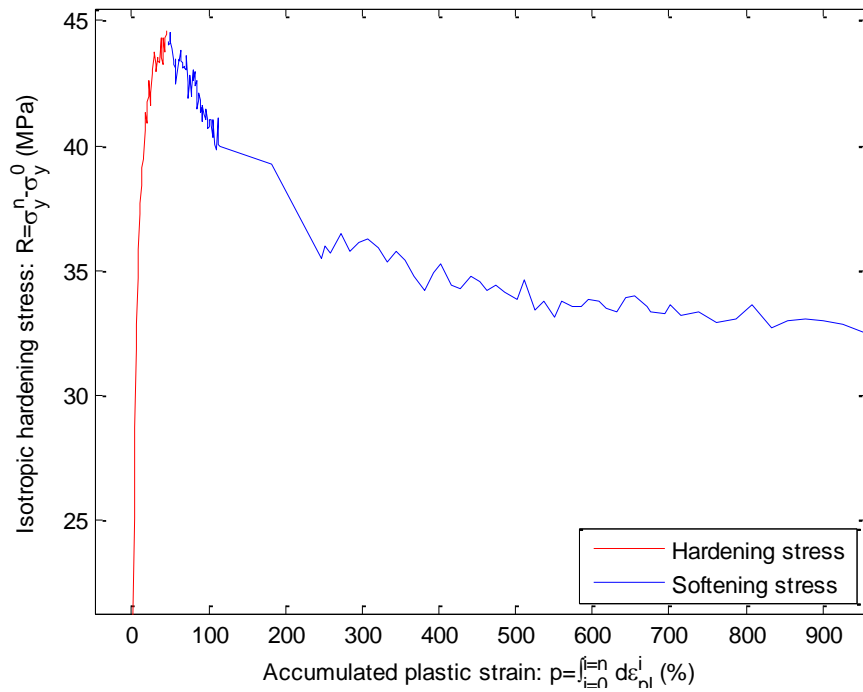


Figure 2.46 Zoomed version of Figure 2.45

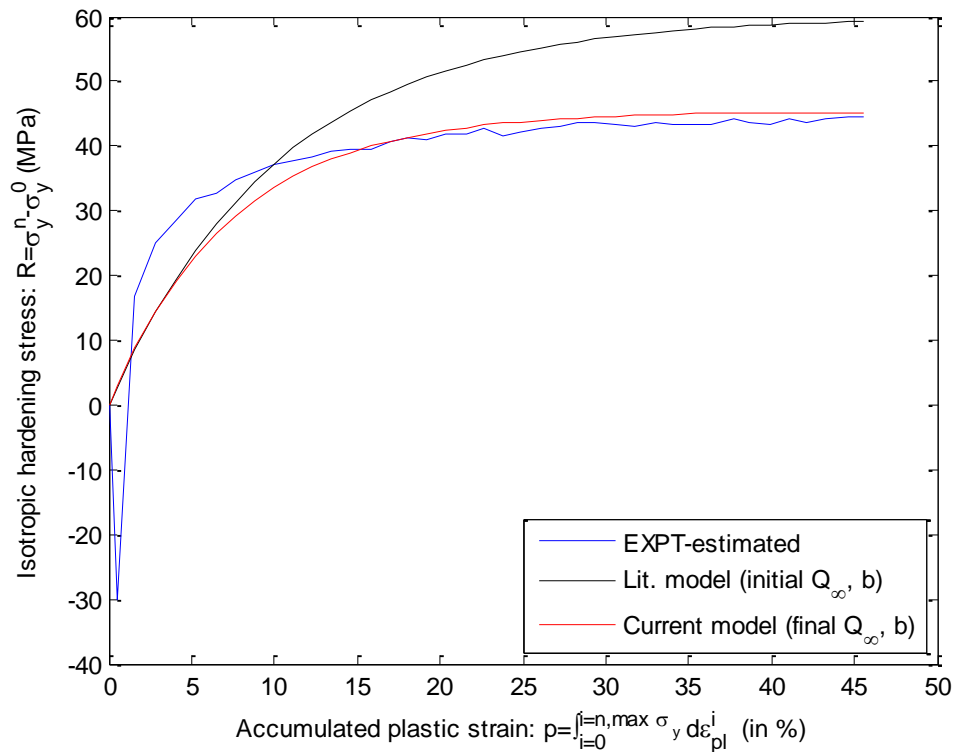


Figure 2.47 Predicted vs. actual isotropic hardening stress

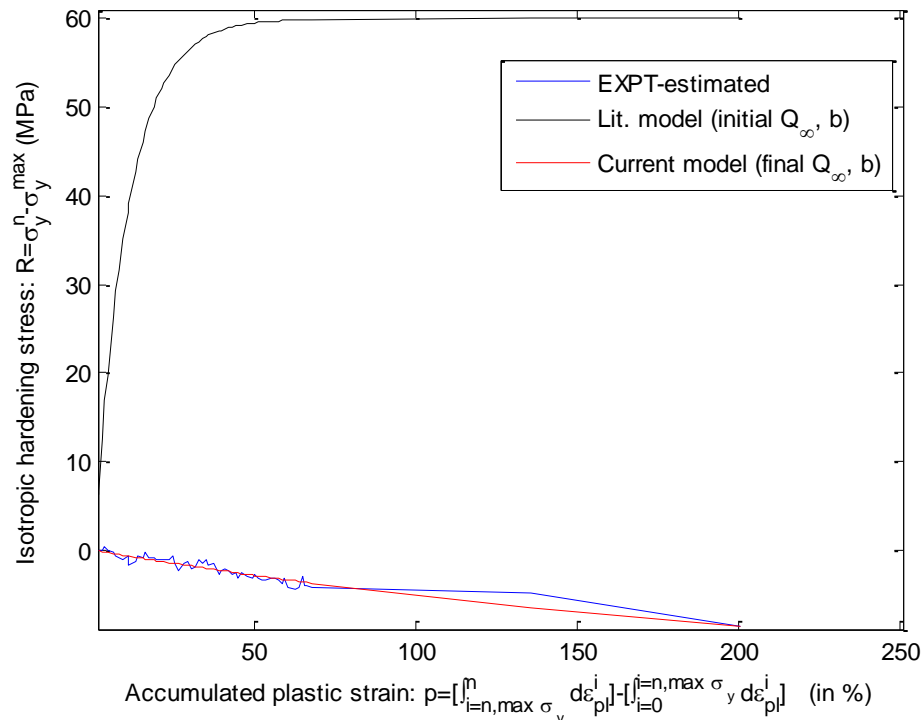


Figure 2. 48 Predicted vs. actual isotropic softening stress (up to first 100 cycles)

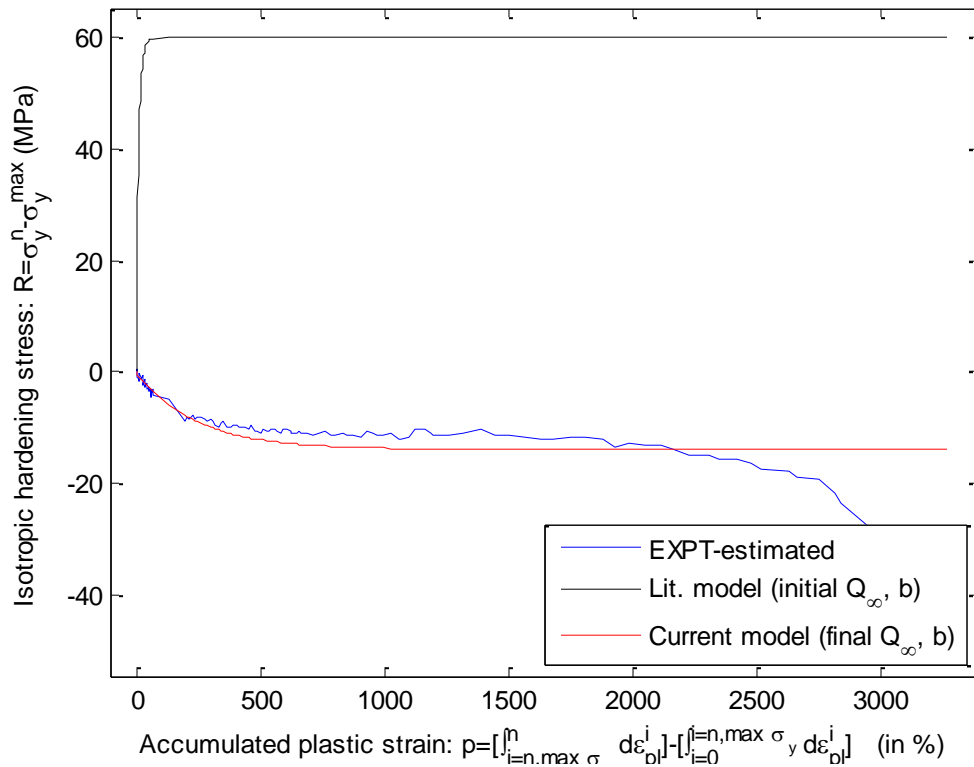


Figure 2. 49 Predicted vs. actual isotropic softening stress (up to 25% load drop cycle of 2602)

Table 2. 1 Estimated isotropic hardening parameters (with assumption of 0.1% offset yield stress) for 316SS under PWR condition

Case type	$Q^{\infty h}$ or $Q^{\infty s}$ (MPa)	b^h or b^s	Gauss-newton Iteration number	$\ \Delta \mathbf{L}\ _2 \leq t_{tol} = 1 \times 10^{-6}$ (refer Eq. 1.17)
Hardening constants up to R^{\max} (refer Eq. 1.10)	45.33	13.556	4261	9.9811e-07
Softening constants from R^{\max} (refer Eq. 1.10) to first 100 cycle	-14.828	0.43257	262	8.9379e-07
Softening constants from R^{\max} (refer Eq. 1.10) to 25% load drop cycle (2602)	-13.88	0.41487	91	5.2586e-07

2.4.4 Evolution of linear kinematic hardening (Prager model) parameters

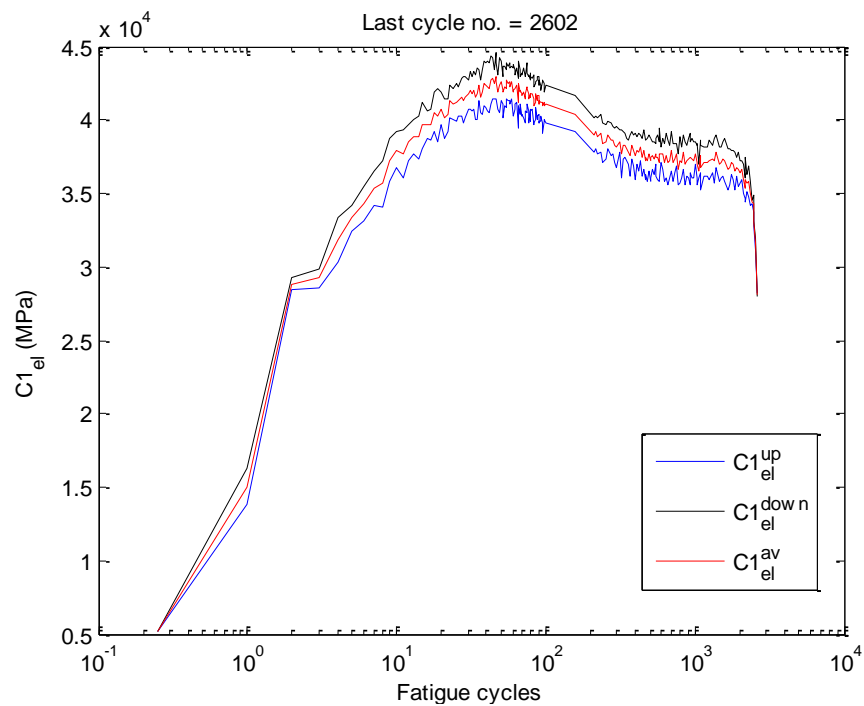


Figure 2. 50 Prager linear kinematic model parameter $C1$ evolution (up to 25% load drop cycle 2602 and with elastic limit stress as offset yield stress) for 316SS under PWR condition

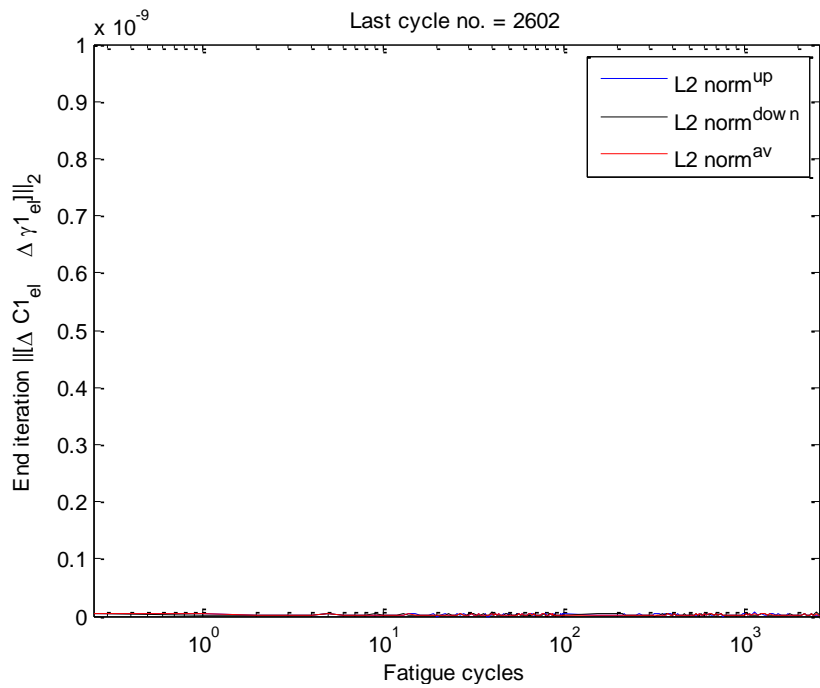


Figure 2. 51 Error norm with respect to fatigue cycle while estimating the Prager linear kinematic model parameters shown in Figure 2.50

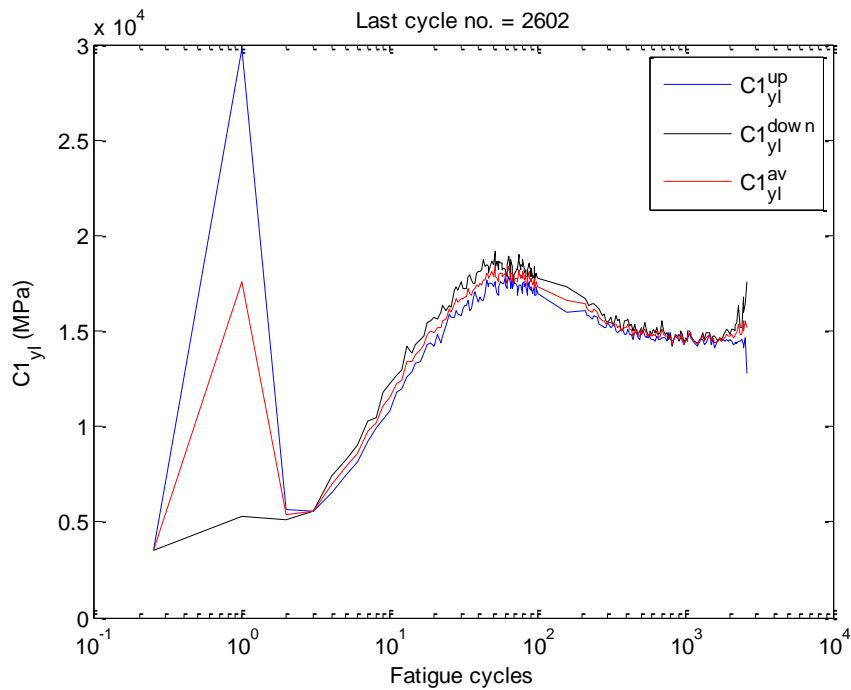


Figure 2. 52 Prager linear kinematic model parameter $C1$ evolution (up to 25% load drop cycle 2602 and with 0.1% offset yield stress) for 316SS under PWR condition

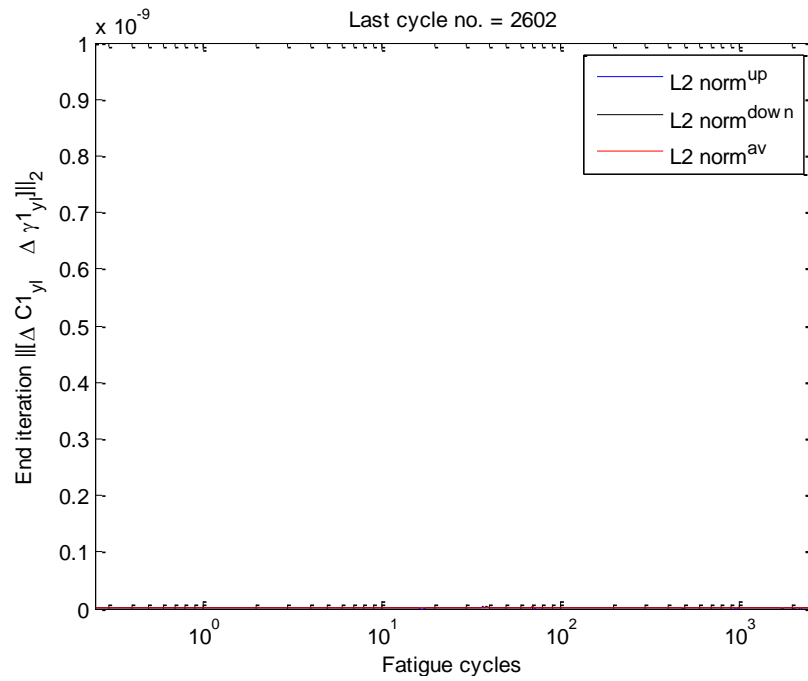


Figure 2. 53 Error norm with respect to fatigue cycle while estimating the Prager linear kinematic model parameters shown in Figure 2.52

2.4.5 Evolution of nonlinear kinematic hardening (Chaboche model) parameters

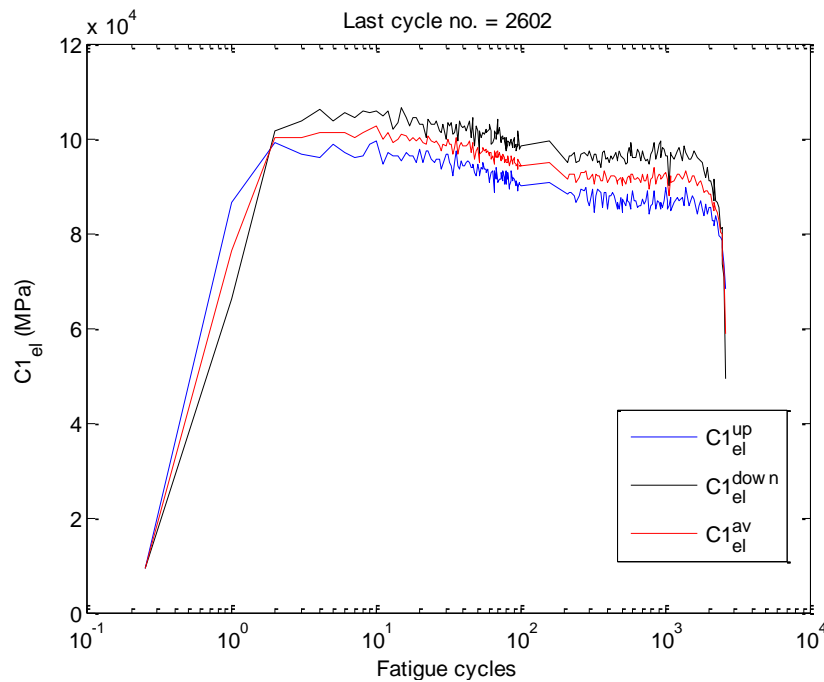


Figure 2. 54 Chaboche kinematic model parameter $C1$ evolution (up to 25% load drop cycle 2602 and with elastic limit stress as offset yield stress) for 316SS under PWR condition

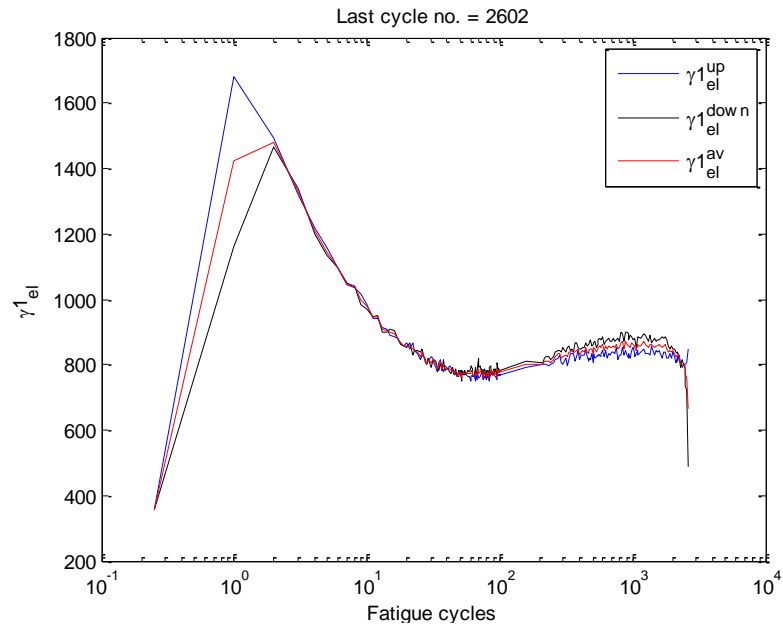


Figure 2. 55 Chaboche kinematic model parameter γ^1 evolution (up to 25% load drop cycle 2602 and with elastic limit stress as offset yield stress) for 316SS under PWR condition

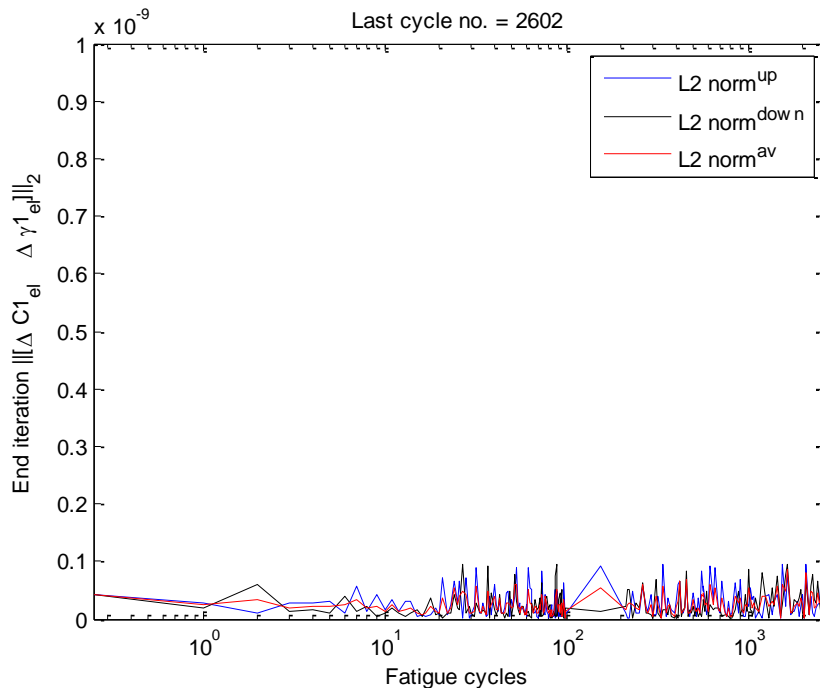


Figure 2. 56 Error norm with respect to fatigue cycle while estimating the Chaboche nonlinear kinematic model parameters shown in Figure 2.54 and Figure 2.55

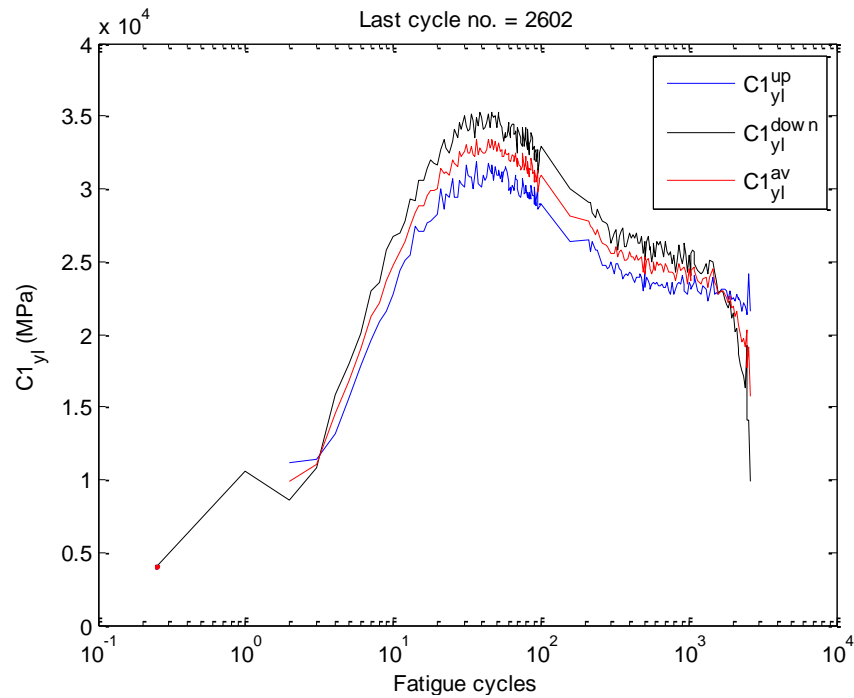


Figure 2. 57 Chaboche nonlinear kinematic model parameter $C1$ evolution (up to 25% load drop cycle 2602 and with 0.1% offset yield stress) for 316SS under PWR condition

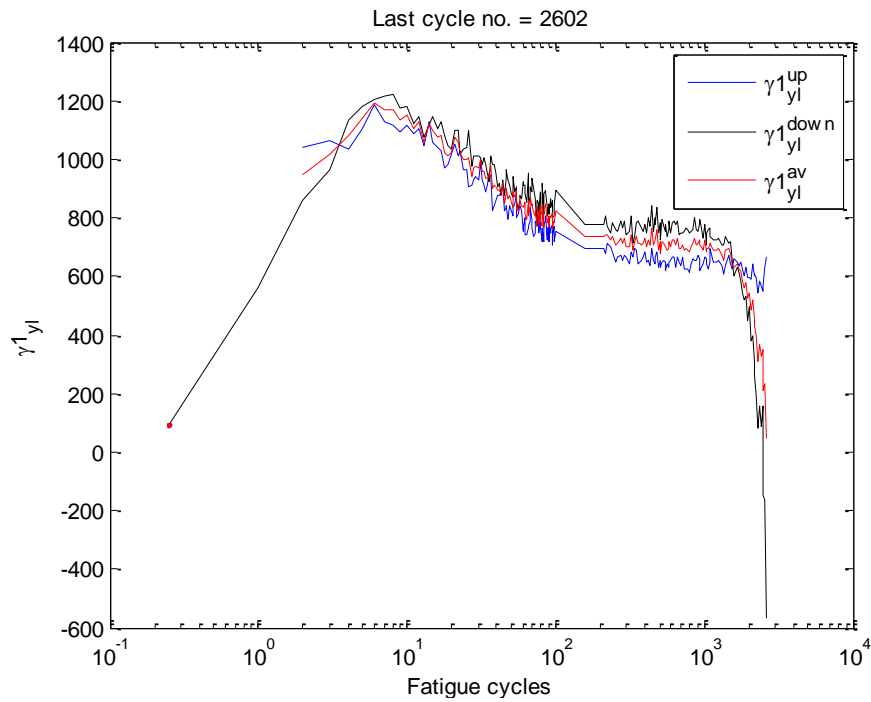


Figure 2. 58 Chaboche nonlinear kinematic model parameter $\gamma1$ evolution (up to 25% load drop cycle 2602 and with 0.1% offset yield stress) for 316SS under PWR condition

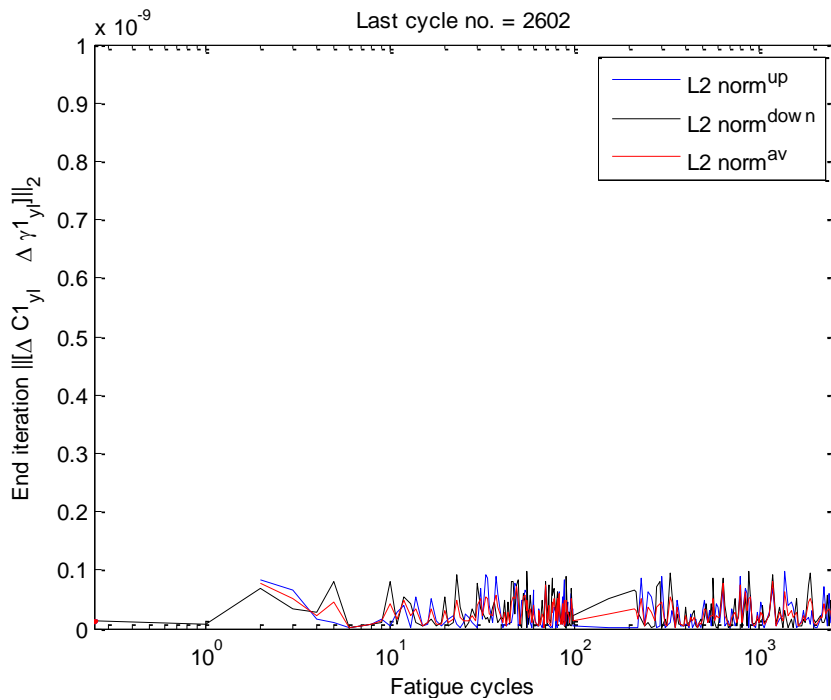


Figure 2. 59 Error norm with respect to fatigue cycle while estimating the Chaboche nonlinear kinematic model parameters shown in Figure 2.57 and Figure 2.58

2.5 Summary

In this Section the following are presented,

- The generic steps involved in the environmental fatigue test procedure are discussed with respect to F14 PWR environment fatigue test.
- With the absence of strain measurements, the stroke measurements were used to predict the corresponding strain.
- The cycle-by-cycle stress-strain data were processed and modeled to estimate the evolution of elastic modulus, elastic limit stress, offset yield stress, isotropic hardening parameters, Prager linear kinematic and Chaboche nonlinear kinematic hardening parameters.
- It is anticipated that these bulk material parameters can be directly used in commercial finite element code for component level cyclic plasticity or fatigue modeling.

This page intentionally left blank



Nuclear Engineering Division

Argonne National Laboratory
9700 South Cass Avenue, Bldg. 208
Argonne, IL 60439

www.anl.gov



Argonne National Laboratory is a U.S. Department of Energy
laboratory managed by UChicago Argonne, LLC